Article:

Jones, RJ, Manville, V orcid.org/0000-0002-0829-1012 and Andrade, D (2015) Probabilistic analysis of rain-triggered lahar initiation at Tungurahua volcano. Bulletin of Volcanology, 77 (8). 68. ISSN 0258-8900

https://doi.org/10.1007/s00445-015-0946-7

Title: **Probabilistic Analysis of Rain-Triggered Lahar Initiation at Tungurahua Volcano**

Authors: Robbie Jones[a,*], Vern Manville[a], Daniel Andrade[b]

Affiliations: [a]University of Leeds, Leeds. LS2 9JT, United Kingdom

[b]Instituto Geofisico, Escuela Politécnica Nacional, P.O. Box 1701-2759, Quito, Ecuador

***Corresponding author:** eerj@leeds.ac.uk

Abstract:

Semi-continuous production of pyroclastic material by intermittent strombolian, vulcanian and sub-plinian eruptions at Volcán Tungurahua, Ecuador has created a persistent rain-triggered lahar hazard during the 1999-present eruptive episode. Lahars threaten the city of Baños, which lies approximately 8 km from the crater, as well as other villages and vital infrastructure situated in close proximity to the dense radial drainage network of the volcano. This study analyses the initiation of rain-triggered lahars and the influence of antecedent rainfall on this process in two northern instrumented drainages, La Pampa and the Vazcun. Analysis of lahar-triggering rainfall intensity and duration between March 2012 and June 2013 yields a power-law relationship, while Receiver Operating Characteristic (ROC) analysis indicates that peak rainfall intensity (10 minute, 30 minute and 60 minute) is the most effective single predictor of lahar occurrence. The probability of a lahar exceeding a pre-defined magnitude increases with peak rainfall intensity. Incorporation of antecedent rainfall (24 hour, 3 day, 5 day and 7 day) as a secondary variable significantly impacts lahar probabilities, particularly during moderate-high intensity rainfall events. The resultant two and three-dimensional lahar probability matrices are applied to rainfall data between 1st July and 31st December 2013 with the aim of predicting lahar occurrence.

Composite lahar indicators comprised from the mean lahar probability estimates of individual matrices are shown to perform this task most effectively. ROC analysis indicates a probability >80% that these composite indicators will generate a higher estimated lahar probability for a randomly selected lahar event than a randomly selected non-lahar event. This method provides an average of 24 minutes of additional warning time compared with the current Acoustic Flow Monitors (AFMs) used for lahar detection, effectively doubling warning times for key downstream infrastructure in the two drainages. Ultimately, this method of lahar analysis could be used to construct real-time probabilistic rain-triggered lahar forecasts as an aid to current lahar hazard mitigation techniques at any location with a significant rain-triggered lahar hazard and a basic instrumental set-up.

1.0 Introduction

Volcán Tungurahua (Lat. 01°28′S; long. 78°27’W) is a 5,023 m high stratovolcano located in the Eastern Cordillera of the Ecuadorian Andes *(Fig. 1)*, lying approximately 120 km south of Quito and 33 km Southeast of Ambato, the capital of Tungurahua Province *(Hall et al. 2013).* The steep-sided edifice features a radial drainage pattern, whilst the Puela, Chambo and Pastaza rivers surround the volcano to the South, West and North respectively. The Pastaza river flows eastwards, past the city of Baños (pop. 18,000), which lies c. 8 km North of the summit of the volcano at an altitude of 1,800 metres above sea level *(Williams et al. 2008; Eychenne et al. 2012; Hall et al. 2013).* Baños is a popular tourist destination and its population increases to as much as 50,000 during holiday periods *(Hall et al. 2013)*. Due to its location, the city (along with surrounding smaller villages) is threatened by numerous hazards from Tungurahua including lahars, pyroclastic density currents (PDCs) and ashfall *(Williams et al. 2008).* This issue is further exacerbated by recent increases in population, infrastructure and economic activity in the region *(Biggs et al. 2010)*. The primary road linking Baños with the Pan-American Highway and other provincial cities crosses several of the lahar-prone northern drainages of Tungurahua; whilst smaller roads which reduce travel times to the large city of Riobamba cross many of the western drainages *(Sorenson et al. 2003).*

Previous lahar-centric studies at Tungurahua have focused on the modelling of single flow events *(Williams et al. 2008).* This contrasts with studies of lahar initiation thresholds over a significant time period such as those undertaken at Mt. Pinatubo *(Arboleda and Martinez 1996; Martinez et al. 1996; Rodolfo et al. 1996; Tungol and Regalado 1996; Van Westen and Daag 2005);* Mt. Mayon *(Rodolfo and Arguden 1991)*; Mt. Merapi *(Lavigne et al. 2000a; Lavigne et al. 2000b)*; Mt. Semeru *(Lavigne and Suwa 2004);* Soufriere Hills *(Barclay et al. 2007);* Volcán de Colima *(Capra et al. 2010);* Sakurajima *(Hikida et al. 2007)* and Yakedake *(Okano et al. 2012).* This study presents an evaluation of the lahar activity within two lahar-prone Northern drainages of Tungurahua between March 2012 and December 2013; with a primary focus on the impacts of antecedent rainfall on the probability of lahar occurrence.

[Figure 1] – Overview Location Map

1.1 Eruptive Activity at Volcán Tungurahua

Since Spanish colonial records began in 1532 AD, Tungurahua has displayed frequent eruptive activity *(Hall et al. 1999)*. There are 17 known distinct eruptions during this timespan, and an average of one major eruptive episode per century. Such major eruptions have occurred in 1640-1641, 1773-1777, 1886-1888, 1916-1918 and 1999-Present and range in composition from basaltic andesite to dacite *(Hall et al. 1999; Le Pennec et al. 2008; Biggs et al. 2010).*

The current period of eruptive activity began in October 1999 after approximately 80 years of dormancy and has featured intermittent strombolian, vulcanian and sub-plinian eruptions *(Eychenne et al. 2012; Hall et al. 2013).* Eruptive products have been predominantly andesitic (58-59% SiO_2) with rare dacitic outbreaks *(Samaniego et al. 2011; Eychenne et al. 2012; Hall et al. 2013)*. This activity (VEI 1-3) has been characterised by lava emissions, tephra falls, PDCs and lahars; with one explosive phase in August 2006 producing PDCs with runout distances of 7.5-8.6 km. These flows reached the base of Tungurahua's edifice and caused six fatalities *(Eychenne et al. 2012; Douillet et al. 2013a; Douillet et al. 2013b; Hall et al. 2013; Bernard et al. 2014).* May 2010 included another explosive eruptive phase featuring PDCs with runout distances of 1-3 *km (Eychenne et al. 2012; Myers et al. 2014)*, whilst more recently eruptive activity in July 2013 and February, April and August 2014 has produced PDCs and ashfall deposits.

1.2 Lahar Background

A lahar is commonly defined as "a rapidly flowing mixture of rock debris and water (other than normal stream flow) from a volcano" *(Smith and Fritz 1989).* Therefore, the term lahar describes a continuum of flow types, often categorised in scientific literature into sub-divisions such as debris flows (>60% sediment by volume), hyperconcentrated flows (20-60% sediment by volume) and streamflows (<20% sediment by volume) *(Fagents and Baloga 2006; Doyle et al. 2010).* Liquid-solid interactions within a lahar can be highly variable on both a spatial and temporal scale due to erosional and depositional processes including bulking (the increase in flow volume by erosion), de-bulking (volume loss by selective deposition), dilution (the increase in flow volume via the interaction with a water source) and infiltration (the loss of liquid into permeable substrates) *(Fagents and Baloga 2006).*

Lahar initiation requires a supply of volcaniclastic material, a source of water, adequate relief and a trigger mechanism. The latter can include crater lake ejection *(Kilgour et al. 2010)*; crater lake breaching *(Manville and Cronin 2007; Massey et al. 2009)*; syn-eruptive melting of ice and snow by PDCs and surges *(Lowe et al. 1986; Major and Newhall 1989; Pierson et al. 1990; Waythomas et al. 2013)*; debris avalanche de-watering *(Cummans 1980)* and rainfall initiation *(Waldron 1967; Rodolfo and Arguden 1991; Major et al. 1996; Rodolfo et al. 1996; Hodgson and Manville 1999; Lavigne and Thouret 2003; Barclay et al. 2007; Capra et al. 2010; Dumaisnil et al. 2010; de Bélizal et al. 2013).* The primary initiation mechanism at Tungurahua is that of rainfall on fresh pyroclastic deposits.

Rain-triggered lahars occur due to a variety of specific mechanisms. These mechanisms include rilling and erosion due to heightened Hortonian overland flow as a result of deposit saturation *(Horton 1945; Collins et al. 1983; Collins and Dunne 1986; Kean et al. 2011)*; as well as shallow landslides (often above an internal detachment surface such as a contact between ash layers) via buoyant support provided by heightened sub-surface water pressure within saturated deposits *(Iverson and Lahusen 1989; Hodgson and Manville 1999; Manville et al. 2000; Crosta and Dal Negro 2003; Zanchetta et al. 2004).* Additional competing processes involved in rain-triggered lahar initiation are those of surface crust formation and rain splash erosion *(Fiksdal 1982;*

Collins et al. 1983; Collins and Dunne 1986; Folsom 1986; Bradford et al. 1987a; Leavesley et al. 1989; Manville et al. 2000). Below a rainfall kinetic energy threshold, rain beat compaction forms a runoff-enhancing surface crust on pyroclastic deposits that enhances Hortonian overland flow and encourages potential lahar formation via sheetwash. Once this rainfall kinetic energy threshold is exceeded the detachment of surface particles by splash erosion becomes the dominant process rather than crust formation *(Wang et al. 2014).* Rain splash erosion of this nature has high erosional potential and whilst it does not decrease deposit infiltration rates like surface crust formation, it does increase the amount of available material that can be easily transported *(Bradford et al. 1987a; Wang et al. 2014)*. Other factors which have been identified as impacting the nature of the rain-triggered lahar hazard include pyroclastic deposit thickness *(Rodolfo and Arguden 1991; Janda et al. 1996; Scott et al. 1996)*, the grain size distribution of the pyroclastic material *(Yamakoshi and Suwa 2000; Ogawa et al. 2007; Craddock et al. 2012)*, deposit volatile content (Waldron 1967), slope angle *(Gómez et al. 2003)*, vegetation coverage *(Yamakoshi and Suwa 2000; Major and Yamakoshi 2005; Alexander et al. 2010)*, vegetation type *(Capra et al. 2010)*, climate *(Lavigne et al. 2007; Okano et al. 2012; de Bélizal et al. 2013)*, the presence of volatile salts and/or hydro-repellent compounds *(Murata et al. 1966; Waldron 1967; Capra et al. 2010)*, and the post-deposition age and experiences of the deposit *(Fiksdal 1982; Major and Yamakoshi 2005)*.

Lahars are a high-frequency hazard at Tungurahua due to high annual rainfall and the frequent eruptive activity which regularly replenishes supplies of loose unconsolidated pyroclastic material on the volcano. This hazard is further enhanced by the steep upper slopes of Tungurahua, which have an average gradient of c. 28^{o} *(Hall et* *al. 2013).* Tungurahua lies in the Intertropical Convergence Zone (ITCZ) and this results in warm, moist air from the Amazon lowlands condensing as it meets the Eastern Cordillera of Ecuador, giving rise to an estimated 3,000 mm of annual rainfall. However, sharp topographic irregularities and high relief in the region produce significant spatial variability and numerous local microclimates *(Garreaud 2009; Le Pennec et al. 2012; Hunink et al. 2014)* so that some high altitude locations receive >6,000 mm yr^{-1} due to enhanced orographic rainfall *(Garreaud 2009)*. Summer precipitation in the region is typically characterised by intermittent *aguaceros* (deluges) between dry periods whilst winter precipitation usually occurs in the form of more sustained *lovizna* (drizzle) that gives larger total rainfall *(Le Pennec et al. 2012).*

2.0 Methods

2.1 Study Region

The Vazcun and La Pampa catchments located on the northern slopes of Volcán Tungurahua are the focus of this study (*Fig. 3)*. The La Pampa catchment (5.07 km^2) covers twice the area of the Vazcun catchment (2.23 km^2). The Vazcun is generally steeper (mean slope 40.4^o versus 31.8^o), but both catchments have a similar maximum gradient (77.0^o and 77.6^o respectively). These two drainages were selected for analysis due to the high frequency of rain-triggered lahars within them, their proximity to human activity and vital infrastructure, and the fact that they are instrumented *(Fig. 3).*

[Figure 2] – Photos of Lahars & Impacts

Following the onset of new eruptive activity in October 1999, the majority of lahars in the La Pampa drainage partially or totally blocked the road between Baños and the Pan-American Highway for hours or even days *(Fig. 2C)*. No injuries or fatalities occurred as a result but several cars have been buried by lahar deposits after failed attempts to cross the La Pampa during the early-stages of flow inundation. In 2008 this issue was alleviated by the construction of a bridge; however large lahars still pose a risk to this vital piece of infrastructure. One of the largest known lahars in the La Pampa catchment occurred on the 10th May 2000, with an estimated peak discharge of 110 m^3s^{-1} and a flow volume of at least $1x10^5$ m^3.

The El Salado Baths are a popular visitor attraction within the Vazcun Valley located approximately 1 km upstream of Baños. These baths host around 300 visitors per day in peak season and on the 12th February 2005 the outer walls were partially destroyed by a large lahar *(Fig. 2) (Williams et al. 2008).* This flow came within tens of centimetres of inundating the baths, had a peak discharge of approximately 100 m^3s^{-1} and an estimated total volume of $5.4\text{-}7x10^4$ m^3 *(Williams et al. 2008).* The El Salado Baths remain a location at risk from lahars in the Vazcun Valley, along with the primary road bridge approximately 1 km further downstream and other structures proximal to the drainage in western parts of Baños.

Acoustic Flow Monitors (AFMs) perform simple signal processing on the ground vibration signals picked up by cheap and robust geophones to detect the passage of lahars [e.g. Pinatubo (Tungol and Regalado 1996); Merapi *(Lavigne et al. 2000b)*; Ruapehu *(Cole et al. 2009)].* There is a network of c. 14 active AFMs around Tungurahua located in 6 different drainages. The Vazcun (VAZ-01) and La Pampa (JUI-01) AFMs utilised in this study (visible in *Fig. 3)* are located at altitudes of 2,455 m and 2,390 m respectively. The Vazcun AFM lies c. 4 km upstream of the primary road crossing (alt. 1,850 m) and 2.9 km upstream of the El Salado Baths (alt. 1,950 m). The La Pampa AFM lies c. 1.9 km upstream of the primary road crossing (alt. 2,000 m). These AFMs register the average amplitude recorded at five minute intervals on a continuous basis. The single telemetered rain gauge on the slopes of Tungurahua is located at an altitude of 2,725 m in the Pondoa region on the Northern slopes of the volcano *(Fig. 3)* and provides rainfall data every 5 minutes at a sensitivity of 0.5 mm.

[Figure 3] – "Birds Eye" GIS View of Vazcun and La Pampa

Tungurahua is monitored from the Tungurahua Volcano Observatory (OVT), operated by the Instituto Geofísico, Escuala Politécnica Nacional (IGEPN) and located approximately 12 km NNW of the crater. In addition to the monitoring at OVT, a community-based monitoring system consisting of a network of volunteers known as *vigias* has existed at Tungurahua since 2000 *(Stone et al. 2014)*. This network currently consists of approximately 35 *vigias* and fulfils multiple risk reduction roles by working collaboratively with both local communities and the scientists at OVT *(Stone et al. 2014)*.

2.2 Datasets

AFMs can yield information regarding flow magnitude via the calibration of output data with visual observations of active flows and their velocity and stage height, assuming that sediment concentration and grain-size distribution are constant. Sequential AFMs along the same channel can indicate the frontal propagation velocity of flows *(Lavigne et al. 2000b; Marchi et al. 2002; Cole et al. 2009).* The sediment concentration and grain-size distribution of flows can also be inferred if broadband seismometers are utilised in conjunction with AFMs *(Burtin et al. 2008; Cole et al. 2009; Kumagai et al. 2009; Zobin et al. 2009; Schneider et al. 2010)*. Debris flows typically peak in the low band (<100 Hz) of AFMs whilst hyperconcentrated flows and streamflows typically peak at higher frequencies *(Marcial et al. 1996; Huang et al. 2004; Cole et al. 2009; Doyle et al. 2009).* The AFMs installed at Tungurahua use L10AR digital exploration geophones with a maximum dynamic range of 3.8x10^{-3} cms^{-1} vertical ground velocity: signal processing produces amplitude measures in low frequency (10-100 Hz), high frequency (100-300 Hz) and full frequency (10-300 Hz) bands.

AFM data at Tungurahua comprises daily spreadsheets containing timestamp, average low band amplitude, average high band amplitude, average full band amplitude and battery functionality at a resolution of five minutes. Rainfall data also consists of daily spreadsheets; containing 5 minute resolution information regarding measured rainfall to a sensitivity of 0.5 mm. Initial data processing involves compilation and synchronisation of Vazcun AFM, La Pampa AFM and Pondoa rain gauge data to enable the initial identification of lahar activity and rainfall events.

2.3 Event Selection

Two primary criteria have been employed to select events for further study. First, if at least 10 mm of rainfall is recorded in a single event at the Pondoa rain gauge then the event will be analysed. A rainfall event is defined in this instance as a period of recorded rainfall between two dry spells of six hours or longer. This minimum inter-event time of six hours is selected due to its frequent use in soil erosion studies *(Wischmeier and Smith 1978; Todisco 2014)* Second, events on the AFM records that feature sustained low band amplitudes of >100 counts for >10 minutes will also be analysed.

A lahar “alert” event occurs when the pre-defined “alert” threshold in the low band signal is exceeded for consecutive recordings (i.e. > 10 minutes). This binary alert system detects lahars with discharges that could pose a potential risk to people and/or infrastructure. During this study period, the threshold values were set by the OVT at 530 for the Vazcun AFM and 500 for the La Pampa AFM, corresponding to currently estimated flow discharges in excess of c. 10-15 m^3s^{-1} and c. 20-25 m^3s^{-1} respectively. This study thus provides a detailed analysis of all rainfall events of ≥10 mm recorded at the Pondoa rain gauge between March 2012 and December 2013; as well as detailed analysis of all significant lahar activity in the Vazcun and La Pampa drainages over the same duration.

3.0 Intensity/Duration (I/D) Analysis

Lahar-triggering rainfall is here defined as "rainfall that includes no pauses longer than 30 minutes and results in a flow that exceeds a pre-defined AFM amplitude" *(Tungol and Regalado 1996);* in this case the pre-defined AFM amplitudes are the *lahar alert* thresholds described above. Analysis of lahar-triggering rainfall duration and lahar-triggering rainfall intensity has been frequently utilised as a means of examining lahar initiation thresholds at many volcanoes; e.g. in the Philippines *(Rodolfo and Arguden 1991; Arboleda and Martinez 1996; Martinez et al. 1996; Rodolfo et al. 1996; Tungol and Regalado 1996; Van Westen and Daag 2005)*, Indonesia *(Lavigne et al. 2000a; Lavigne et al. 2000b; Lavigne and Suwa 2004),* Mexico *(Capra et al. 2010)*, Montserrat *(Barclay et al. 2007)* and Japan *(Hikida et al. 2007; Okano et al. 2012)*. This analysis typically produces a power-law relationship suggesting lahar initiation occurs along a continuum from short duration, high intensity rainfall events to long duration, low intensity events.

[*Figure 4]- I/D Plot with Tungurahua Lower and Upper Bounds + Other Locations*

Fig. 4 illustrates this relationship for 23 of 29 lahar alert events within the Vazcun and La Pampa drainages of Tungurahua between March 2012 and June 2013 associated with triggering rainfall recorded at the Pondoa rain gauge. Six lahar alerts (20.7%) occurred with no detected triggering rainfall at the Pondoa rain gauge and were omitted from the analysis. These six lahar alerts highlight the spatial variability of rainfall around Tungurahua and the potential limitations of the single telemetered rain gauge. Of the remaining lahar alerts, 82.6% plot between a lower boundary curve of $I=1.1D^{-0.75}$ and an upper boundary curve of $I=5D^{-0.75}$.

4.0 Receiver Operating Characteristic (ROC) Analysis

The I/D analysis method does not take into account factors such as antecedent rainfall magnitude and eruptive activity that could impact both rainfall-runoff relationships and sediment availability, potentially affecting the rainfall thresholds required to initiate lahars of a given magnitude. Here, the influence of these factors is investigated using Receiver Operating Characteristic (ROC) analysis within the IBM SPSS statistics software package. ROC analysis is a common diagnostic test that was first utilised during World War Two to assess the ability of radar systems to differentiate between noise and signals associated with enemy planes *(Swets et al. 1988)*. This method illustrates the performance of a binary classifier system as different contributing instances are assessed *(Fawcett 2006).* In this case, the binary classifier system is the presence (or lack) of a lahar alert during a rainfall event of 10 mm or above. ROC analysis is used to investigate the sensitivity of lahar alert occurrence in the

Vazcun and La Pampa drainages to potential contributing variables between March 2012 and June 2013. These variables are total event rainfall, peak rainfall intensity, antecedent rainfall, number of recorded explosions and elapsed time since last reported PDC activity. In order to apply this analysis technique to lahars at Tungurahua the potentially contributing factors need to be defined and quantified.

Total Event Rainfall is defined as the rainfall recorded between two dry periods of ≥6 hours. Rainfall events featuring ≥10 mm of total rainfall are utilised in the ROC analysis; with total rainfall recorded at a resolution of 0.5 mm.

Peak rainfall intensity (mm/min) is defined as the maximum rainfall intensity value recorded by the Pondoa rain gauge during the same rainfall event that produced the relevant lahar alert. Rainfall intensity is analysed during all rainfall events ≥10 mm and is recorded at a time resolution of five minutes for three rainfall intensity time scales; *60 minutes, 30 minutes and 10 minutes*.

Antecedent rainfall is calculated for each analysed rainfall event at a resolution of 0.5 mm. Four antecedent rainfall timescales are recorded; 24 hours, and 3, 5 and 7 days. In the case of a lahar alert event the antecedent rainfall is calculated for the period preceding the onset of the relevant rainfall event.

In order to analyse the relationship between renewed sediment supply and lahar occurrence an eruptive activity timeline for the data period was created from the daily activity reports published by IGEPN. These reports contain information on long-period, volcanic-tectonic and tremor seismicity, number of explosions, visibility level, evidence of ash fall, observed plume height, wind direction, evidence of PDC activity and runout distance/direction of PDCs. Due to its reliance on qualitative observations the volume of information available varies on a daily basis.

(Figure 5) - Timeline

Fig. 5 illustrates the potential use of such a timeline by displaying *time since last PDC activity* and *daily recorded explosions* at Tungurahua as potential proxies for eruptive activity and thus sediment supply. This timeline also features daily rainfall and the timing of lahar alert events between March 2012 and June 2013 *(Fig. 5)*. *Fig. 5* does not visually suggest that the upper catchments of the Vazcun and La Pampa drainages are sediment limited, with lahar alerts occurring throughout the data period during high magnitude rainfall events; irrespective of the timing of eruptive activity. *Explosion frequency* over 5 different timescales (24 hours, 3 days, 7 days, 30 days and 60 days) and time since last reported PDC activity are used in the ROC analysis as proxies for sediment supply in an attempt to statistically analyse the impacts of the eruptive cycle upon lahar alert occurrence.

The primary graphical output of ROC analysis is called a ROC curve *(Fig. 6)*. Such curves plot the percentage of true positives against the percentage of false positives for each possible diagnostic threshold value *(Swets et al. 1988; Fawcett 2006)*. The ROC curve of a perfect diagnostic test would begin in the lower left corner of a plot, go straight up to the upper left corner, and then to the upper right corner; indicating that it is both 100% *sensitive* and 100% *specific (Swets et al. 1988; Fawcett 2006)*. Conversely, a random test with correct diagnosis odds of 50/50 would theoretically produce a diagonal line from the lower left corner to the upper right corner. The effectiveness of diagnostic tests can thus be compared by evaluating the area of the graph which lies under the ROC curve; a perfect test producing an area of 1 and a random test producing an area of 0.5 *(Swets et al. 1988; Fawcett 2006)*.

4.1 ROC Curves

[Figure 6$_{abcd}$] – ROC Curves & Stats

Fig. 6a displays lahar alert centric ROC curves for the three peak rainfall intensity timescales (10, 30 and 60 minutes) and total event rainfall, *fig. 6b* displays lahar alert centric ROC curves for four antecedent rainfall periods (24 hour, 3, 5 and 7 days) and time since last PDC activity, whilst *fig. 6c* displays lahar alert centric ROC curves for reported explosion frequency over the 5 timescales ranging from 24 hours to 60 days. The three peak rainfall intensity timescales (ROC areas >0.8), and to a lesser extent total event rainfall (ROC area >0.76), are the most effective independent predictors of lahar alert occurrence *(Fig. 6a).* All four of these variables achieve statistical significance at a level >99%. Conversely, antecedent rainfall, explosion frequency and time since last PDC activity show no relationship with lahar alert occurrence (i.e. they plot close to the diagonal reference line representing a random relationship) *(Fig. 6b, c)*.

5.0 Probabilistic Analysis

[Figure 7] – 2D Probability Plots for 10, 30 and 60 Minute Peak Rainfall Intensity

Probabilistic analysis of lahar alert occurrence is a potentially useful tool for lahar hazard mitigation. ROC analysis indicates that the best individual indicator of lahar alert occurrence is peak rainfall intensity *(Fig. 6)* and therefore this variable is utilised to investigate lahar alert probability. *Fig. 7* displays the variation in lahar alert probability as peak rainfall intensity increases for rainfall events ≥10 mm (n = 99, of which 30 were associated with 44 separate periods of lahar alert). The 10 mm rainfall event analysis criterion excludes 2 lahar alert-producing rainfall events: i.e. 6.25% of rainfall events that produced a lahar alert signal did not exceed our rainfall event threshold (≥10 mm of rain) in the Vazcun and La Pampa drainages between March 2012 and December 2013.

[Figure 8] – 3D Probability Plots of Lahar Alert Occurrence

Several previous studies have suggested that high levels of antecedent rainfall functions to saturate deposits, increase runoff and thus lower the rainfall required to trigger lahars *(Lavigne et al. 2000a; Barclay et al. 2007; Okano et al. 2012)*. Therefore, high antecedent rainfall would be expected to increase lahar probability across a whole spectrum of rainfall conditions. Despite displaying little correlation with lahar alert occurrence when utilised as a single variable during ROC analysis *(Fig. 6)*, antecedent rainfall has a significant impact when used as a secondary variable in combination with peak rainfall intensity at Tungurahua *(Fig. 8)*. In the three-dimensional probability plots in *fig. 8*, lahar alert probability increases when antecedent rainfall is increased, but only during mod-high peak rainfall intensity events. At low peak rainfall intensities the lahar probability is relatively unaffected by antecedent rainfall impacts. This pattern could be explained by two mechanisms. Firstly, the infiltration rates of Tungurahua eruptive deposits may remain sufficiently high, even after significant antecedent rainfall, to prevent lahar triggering runoff during low intensity rainfall, but not during moderate and high rainfall intensity events. Secondly, antecedent rainfall could increase the bulking efficiency of lahars due to higher water content in channel floor deposits: low-intensity rainfall fails to trigger lahars regardless of channel saturation, but moderate-high intensity rainfall-triggered lahars more readily grow to a level where they trigger an alert. Increased bulking efficiency under high antecedent rainfall conditions is attributed to the development of positive pore pressures in saturated channel floor sediments as the flows pass over them *(Iverson et al. 2010; Reid et al. 2011)*, promoting progressive bed scour, introducing additional fluid to the lahar, and preventing fluid loss from the flow into the channel floor *(Kean et al. 2011)*. In summary, we infer in this specific case that increased antecedent rainfall does not reduce lahar initiation thresholds; instead it acts only to increase lahar alert probability at high rainfall intensities.

6.0 Predicting Events – "Real-time" Lahar Forecasting

As a test of the utility of using the two and three-dimensional probability matrices displayed in *figs. 7 & 8* as a tool to predict lahar alert probability using "real-time" rainfall data, we examined the rainfall record between 1st July and 31st December 2013. As this time period is included in the construction of *figs. 7 & 8* (comprised of 99 ≥10 mm rainfall events between 1st March 2012 and 31st December 2013) each rainfall event is analysed using probability matrices constructed from the other 98 rainfall events in order to minimise bias. The optimal method for this testing would use probability matrices constructed from all events that had occurred prior to the test-event; however due to the limited size of the dataset and considering the relatively constant lahar hazard at Tungurahua, all 98 other rainfall events are used to construct the probability matrices in order to maximise the amount of information in the subsets of each matrix *(Druzdzel and van der Gaag 2000)*. All ≥10 mm rainfall events in the test period were analysed to estimate the associated lahar alert probability and then our predicted lahar alert catalogue *(Table 1)* was compared with the actual lahar alert record.

[Figure 9] – Single Real-time event. December 20th 2013.

For example, a single rainfall event on 20th December 2013 produced a lahar alert signal in the La Pampa drainage *(Fig. 9)*. Calculated lahar alert probability goes up as peak rainfall intensity increases with time during the rainfall event *(Fig. 9)*. Significantly, peak estimated lahar alert probability for each of the three displayed matrices occurs prior to triggering of the (AFM-derived) lahar alert signal by the flow itself. Calculated peak lahar alert probability estimates for all ≥10 mm rainfall events between 1st July and 31st December 2013 are displayed in *Table 1*. Comparison with the actual lahar alert record enables the performance of the two and three-dimensional probability matrices to be assessed using ROC analysis.

[Table 1] – Matrix of Peak Probability Estimates for July-December 2013 Rainfall Events

Each column in *table 1* is analysed relative to the *real-life* occurrence or non-occurrence of lahar alert signals during the 30 featured rainfall events between 1st July and 31st December 2013. ROC curves and associated statistics *(Table 2)* describing the performance of each set of peak estimated lahar alert probabilities are generated and a selection of these curves are displayed in *Fig. 10.* Results show mixed performance by the individual probability matrices shown in columns A-P of *table 1.* Several matrices achieved ROC curve areas >0.8 and statistical significance at a level of 95% (*p*-value ≤0.05), displaying effective lahar prediction, whilst other individual matrices performed less effectively over the test period. The performance of the "composite" lahar indicators (composed of the mean probability outputs of multiple individual probability matrices) displayed in columns P-Y of *table 1* was more consistently effective. 90% of these composite indicators achieved statistical significance at a level of 95% and they produced ROC curve areas ranging from 0.71 to 0.89 with a mean value of 0.80.

[Figure 10] – Selected ROC curves assessing the performance of probability matrices

[Table 2] – ROC Curve Statistics

The timing of the calculated peak lahar alert probabilities is also important, in addition to the performance of the probability matrices in predicting lahar alerts. This method of probabilistic analysis only provides a significant advance over the real-time AFM outputs if it consistently predicts potential lahars *before* such flows are detected by AFMs. *Table 3* considers the 8 known lahar alert signal events that took place between 1st July and 31st December 2013 and assesses the time of peak estimated probability relative to the initial generation of the lahar alert signal. The mean additional warning time per matrix type ranges from 17 minutes to 36 minutes with a mean value of 24.5 minutes, whilst 75% of the tested lahar alert events featured a mean additional warning time of >20 minutes *(Table 3)*. Lahar transit times between the La Pampa AFM and the primary road bridge crossing the drainage are currently estimated at 14±2 minutes, whilst in the Vazcun this value is estimated at 19±2 minutes.

[Table 3] – Table describing peak probability time vs. lahar alert signal occurrence

7.0 Discussion

7.1 Rainfall I/D Analysis

Initial analysis of lahar alert triggering rainfall in the Vazcun and La Pampa drainages of Tungurahua indicated a power-law relationship between lahar-triggering rainfall intensity and duration. This is in common with previous studies of rain-triggered mass-flow events in disturbed earth systems, such as other active volcanoes *(Rodolfo and Arguden 1991; Arboleda and Martinez 1996; Tungol and Regalado 1996)*. The majority of lahar alerts analysed at Tungurahua between March 2012 and June 2013 plotted within a region bounded by the curves $I=1.1D^{-0.75}$ (lower boundary) and $I=5D^{-0.75}$ (upper boundary) *(Fig. 4)*. The coefficients of the power-law relationship vary from volcano to volcano, likely as a function of a range of factors including the grain-size distribution of the pyroclastic material covering the flanks of the volcano. The relatively high position of the Mayon curve in *fig. 4* is probably due to the relatively high infiltration levels at Mayon as a result of the comparatively coarse, granular and porous volcaniclastic surface materials present on the slopes of the volcano *(Rodolfo and Arguden 1991).* The three lower boundary curves at Pinatubo (Sacobia & Pasig-Potrero) and Tungurahua display relatively similar, overlapping thresholds, possibly due to finer ash, lower surface infiltration rates, and thus heightened surface runoff. Furthermore, the definitions of 'triggering rainfall' in *Tungol and Regalado (1996) ,Rodolfo and Arguden (1991), Arboleda and Martinez (1996),* and this study differ. The definition of a "lahar event" also varies; *Rodolfo and Arguden (1991)* pick events subjectively judged to have reached debris flow status; *Arboleda and Martinez (1996)* and *Tungol and Regalado (1996)* use events which exceed a low band AFM value of 100 (estimated at 25 m^3s^{-1}); and this study uses events that trigger a lahar alert signal (estimated at >10-

15 m^3s^{-1} in the Vazcun drainage and >20-25 m^3s^{-1} in the La Pampa). All of these factors preclude I/D relationships derived at one volcano from being applied at another. Furthermore, in addition to the lack of standardisation within the process, the intensity/duration method is of limited use for real-time lahar prediction due to an inability to predict the likelihood of a lahar under any given set of rainfall parameters *(Fig.4)*. Incorporating "non-lahar" events into analytical methods in order to generate lahar alert probabilities is potentially a more valuable method from a lahar forecasting perspective.

7.2 ROC Analysis

The initial aim of the probabilistic lahar alert analysis was to identify the key indicators of lahar alert occurrence. The ROC curves displayed in *fig. 6* indicate that peak rainfall intensity is the most accurate independent indicator of lahar alert occurrence. Conversely, antecedent rainfall, explosion frequency and time since last PDC activity are shown to be ineffective when used as independent indicators of lahar alert occurrence.

Rainfall event magnitude (ROC curve area of 0.76) also displays statistically significant (>99%) correlation with lahar alert occurrence, but to a lesser degree than peak rainfall intensity. This indicates that peak rainfall intensity is more effective than total volume of rainfall in predicting lahars large enough to trigger lahar alerts. From a physical viewpoint, short timescale, high-intensity rainfall may be more likely to overwhelm deposit infiltration capacity and generate lahar-forming surface run-off. Rainfall event magnitude (i.e. total rainfall) fails to make a distinction between low intensity rainfall events which may not overcome such an infiltration rate threshold and higher intensity rainfall events which have the potential to do so.

The importance of short term peak rainfall intensity relative to total rainfall in predicting lahar alerts highlights several potentially important competing processes. As discussed in the introduction, surface crust formation due to rain beat compaction of fine eruptive material has been well documented at a number of volcanoes *(Leavesley et al. 1989; Pierson et al. 1996; Manville et al. 2000; Yamakoshi and Suwa 2000).* This crust is often initially formed during post-deposition periods of high intensity rainfall, reducing infiltration rates and increasing surface runoff, thus heightening the potential for rain-triggered lahars *(Yamakoshi and Suwa 2000).* This process competes with rain splash erosion, which disrupts surface crusting once a rainfall kinetic energy threshold is exceeded, increasing the amount of material available for transport by Hortonian overland flow but also exposing more permeable substrates *(Bradford et al. 1987b; Wang et al. 2014).* Rill formation similarly exposes more permeable substrates to subsequent rainfall events, but also yields additional sediment *(Leavesley et al. 1989)*. This dynamic between surface crusting of deposits, rain splash erosion and rill network formation plays an important role in lahar initiation *(Leavesley et al. 1989; Yamakoshi and Suwa 2000).* Despite the potential of this cyclical process to create temporal and spatial variation in surface infiltration rates, peak rainfall intensity is shown by the ROC analysis to perform consistently well as an independent indicator of lahar alert occurrence in the Vazcun and La Pampa drainages at Tungurahua.

7.3 Probabilistic Analysis & ***Real-Time*** Forecasting

The probabilistic analysis of lahar alert occurrence displays the increasing probability of a lahar alert as peak rainfall intensity (10 minute, 30 minute and 60 minute) increases *(Fig. 7),* as well as the impacts of antecedent rainfall upon these probabilities *(Fig. 8)*. This probabilistic analysis enables the calculation of an evolving lahar alert probability if the database is updated in real-time. It also enables the analysis of different time periods within the overall database; aiding assessment of temporal changes in lahar initiation thresholds and thus lahar occurrence probabilities. Such temporal changes can be due to catchment disturbances as a result of eruptive activity or landslides, fluctuations in sediment availability and seasonal meteorological variations impacting rainfall type and frequency.

The method also acknowledges the uncertainty associated with rain gauge location and meteorological variability. The telemetered Pondoa rain gauge at 2,725 m on the Northern slopes of Tungurahua lies c. 1,300 m below the estimated “lahar initiation region”. As such there is likely to be significant spatial and temporal variation in rainfall between the two locations: i.e. 6 lahar alerts between March 2012 and December 2013 were not associated with any recorded triggering rainfall at the Pondoa gauge. A denser network of rain gauges at a variety of altitudes would aid the identification and reduction of uncertainty between actual and recorded rainfall. This rainfall variation is prevalent at Tungurahua due to the steep slopes, high relief and topographic irregularities. Orographic rainfall in particular could be more effectively captured if high altitude (>4000 m) rain gauges were installed; however this would not be a cost effective measure given the likely lifespan of such instruments.

A probabilistic approach acknowledges the possibility of lahar occurrence when low rainfall intensities are recorded at the rain gauge as well as the potential for lahar absence when high rainfall intensities are recorded. This emphasises the potential benefit of simultaneously using multiple techniques for lahar hazard mitigation, with probabilistic lahar forecasting offering heightened warning times and the AFM network acting as a *failsafe* whilst also yielding additional information regarding specific lahar magnitudes and timing. With such an approach there is the potential for the occurrence of false alarms. Volcanology frequently exhibits the complexity of managing potentially high-impact hazards with variable probabilities and therefore the balance between issuing warnings and being concerned about false alarms is challenging *(Donovan et al. 2014)*. At Tungurahua this balance would rely upon the effective performance of the lahar probability matrices, the AFM network and the community-based volcano monitoring of the vigía network. Vigías living near major lahar-prone valleys have previously been given motorbikes by Civil Defense so that they can check for lahars during rainfall whilst as a network they also act as a communication channel for increasing community awareness (Stone et al. 2014). Therefore they would act as a key component in both the early identification of any potential false alarms and in enhancing understanding within the communities as to why such false alarms could occur.

In order to test the lahar alert probability matrices in real-time, two and three-dimensional probability matrices were applied to the rainfall record between 1st July and 31st December 2013. Assessment of the performance of the lahar alert probability matrices was achieved via ROC analysis of the peak output probabilities of each matrix relative to the actual lahar alert record during this time span (*Table 1*). The results of this forecasting exercise show that dynamic lahar alert probability matrices based on peak rainfall intensity and antecedent rainfall have the potential to effectively predict lahar alert occurrence in conjunction with real-time rainfall data at Tungurahua. Effectiveness is improved when the output peak lahar probability estimates of different probability matrices (based on various timescales of peak rainfall intensity and antecedent rainfall) are combined and averaged to form a composite indicator of potential lahar occurrence. In addition to the effective prediction of lahar occurrence, only one significant false alarm (30/11/13) occurred during this 6 month test period.

The timing of the peak lahar probability estimated from rainfall data relative to the generation of an AFM lahar alert signal is also important for assessing the potential applications of the method *(Table 3)*. Lahar prediction from rainfall data effectively doubles warning times based on AFM lahar alert signals alone in the Vazcun and La Pampa drainages. Automation of probabilistic analysis of real-time telemetered rainfall data at Tungurahua could act as an accurate first-stage lahar warning system at *OVT* for IGEPN, backed up by second-stage AFM alerts (event confirmation or failsafe), in addition to the community-based monitoring of the vigía network.

8.0 Conclusions

Investigation of rain-triggered lahars in two northern drainages of Tungurahua showed a power-law relationship between rainfall intensity (I) and duration (D), in common with previous studies at other active volcanoes and wild-fire impacted watersheds. 82.6 % of lahar events occur between a lower boundary of $I=1.1D^{-0.75}$ and an upper boundary of $I=5D^{-0.75}$.

ROC analysis demonstrated that peak rainfall intensity (10 minute, 30 minute and 60 minute) is the most effective predictor of lahar alert occurrence, while antecedent rainfall magnitude, explosion frequency and time since last known PDC activity have no value as independent indicators of lahar alert occurrence. Probabilistic analysis of all rainfall events of ≥10 mm confirmed this relationship for multiple peak rainfall intensity timescales, with escalating 10 minute, 30 minute and 60 minute peak rainfall intensities demonstrating an increase in lahar alert probability.

Antecedent rainfall was shown to have significant impacts upon lahar alert probability when used as a secondary variable in conjunction with peak rainfall intensity, increasing lahar alert probabilities at moderate-high peak rainfall intensities but not during low intensity rainfall events. Increased antecedent rainfall does not appear to reduce lahar initiation thresholds, due to relatively high saturated infiltration rates on the upper edifice of Tungurahua, but rather increases lahar alert probability during moderate- high intensity rainfall events by increasing flow bulking efficiency through entrainment of saturated channel deposits. Tungurahua does not appear to be sediment-limited with respect to lahar initiation, with flows occurring consistently during the study period of March 2012-December 2013 irrespective of the cycle of eruptive activity.

Application of two and three dimensional probability matrices to real-time rainfall data between 1st July and 31st December 2013 displayed the potential to predict lahar alert occurrence at a high level of confidence. Furthermore, lahar prediction based on composite indicators created from the mean values of multiple probability matrices yielded more reliable lahar warnings than the individual matrices. The matrix derived peak lahar probabilities yielded significantly earlier warnings than the AFM-based lahar alert signals, producing average additional warning times of over 24 minutes per event. Lahar transit times between the La Pampa and Vazcun AFMs and the primary road crossing of each drainage are estimated at 14±2 minutes and 19±2 minutes respectively. As such, this method displays the potential to significantly increase effective lahar warning times.

This study illustrates a probabilistic method of lahar analysis that could be used as a tool in lahar hazard mitigation at any location where rain-triggered lahars present a hazard. Currently, lahar warning systems typically depend on the exceedance of a single pre-defined AFM amplitude. Calibration of AFM records with visual observations of flow volumes, discharges, velocities and sediment concentrations can refine lahar detection to produce multiple AFM thresholds correlated with different peak discharges and/or flow properties. The addition of multiple flow magnitude thresholds into this probabilistic method could assist in the effective modelling of potential flow inundation and arrival times. Despite the low false alarm generation rate during the 6 month test period uncertainty remains regarding the disparity between recorded rainfall at the Pondoa rain gauge and actual rainfall in the lahar initiation region. Further work on the spatial variation of rainfall at the volcano would test the strength of the Pondoa rain gauge as a single data source from which to make effective lahar predictions.

Acknowledgments

The authors are extremely grateful to IGEPN for their support with this research. The authors would also like to thank two anonymous reviewers whose comments helped to improve the manuscript. The research was funded as part of a STREVA (NERC/ESRC consortium project) PhD Studentship.

References:

Alexander J, Barclay J, Susnik J, Loughlin SC, Herd RA, Darnell A, Crosweller S (2010) Sediment-charged flash floods on Montserrat: The influence of synchronous tephra fall and varying extent of vegetation damage. Journal of Volcanology and Geothermal Research, 194:127-138; Doi: 10.1016/j.jvolgeores.2010.05.002

Arboleda R, Martinez M (1996) 1992 Lahars in the Pasig-Potrero River System. In: Newhall C, Punongbayan R (eds) Fire and Mud, Eruptions and Lahars of Mt Pinatubo, Philippines. PHIVOLCS/University of Washington Press, Quezon City/Seattle, pp 1045-1055

Barclay J, Alexander J, Susnik J (2007) Rainfall-induced lahars in the Belham Valley, Montserrat, West Indies. Journal of the Geological Society, 164:815-827; Doi: 10.1144/0016-76492006-078

Bernard J, Kelfoun K, Le Pennec JL, Vargas SV (2014) Pyroclastic flow erosion and bulking processes: comparing field-based vs. modeling results at Tungurahua volcano, Ecuador. Bulletin of Volcanology, 76; Doi: 10.1007/S00445-014-0858-Y

Biggs J, Mothes P, Ruiz M, Amelung F, Dixon TH, Baker S, Hong SH (2010) Stratovolcano growth by co-eruptive intrusion: The 2008 eruption of Tungurahua Ecuador. Geophysical Research Letters, 37; Doi: 10.1029/2010gl044942

Bradford JM, Ferris JE, Remley PA (1987a) Interrill Soil Erosion Processes: I. Effect of Surface Sealing on Infiltration, Runoff, and Soil Splash Detachment. Soil Sci Soc Am J, 51:1566-1571; Doi: 10.2136/sssaj1987.03615995005100060029x

Bradford JM, Ferris JE, Remley PA (1987b) Interrill Soil Erosion Processes: II. Relationship of Splash Detachment to Soil Properties. Soil Sci Soc Am J, 51:1571-1575; Doi: 10.2136/sssaj1987.03615995005100060030x

Burtin A, Bollinger L, Vergne J, Cattin R, Nabelek JL (2008) Spectral analysis of seismic noise induced by rivers: A new tool to monitor spatiotemporal changes in stream hydrodynamics. J Geophys Res-Sol Ea, 113; Doi: 10.1029/2007jb005034

Capra L, Borselli L, Varley N, Gavilanes-Ruiz JC, Norini G, Sarocchi D, Caballero L, Cortes A (2010) Rainfall-triggered lahars at Volcán de Colima, Mexico: Surface hydro-repellency as initiation process. Journal of Volcanology and Geothermal Research, 189:105-117; Doi: 10.1016/j.jvolgeores.2009.10.014

Cole SE, Cronin SJ, Sherburn S, Manville V (2009) Seismic signals of snow-slurry lahars in motion: 25 September 2007, Mt Ruapehu, New Zealand. Geophysical Research Letters, 36; Doi: 10.1029/2009gl038030

Collins B, Dunne T, Lehre A (1983) Erosion of tephra-covered hillslopes North of Mount St. Helens, Washington: May 1980-May 1981 Zeitschrift für Geomorphologische Naturwissenschaftliche Forschung, 16:103-121;

Collins BD, Dunne T (1986) Erosion of Tephra from the 1980 Eruption of Mount St Helens. Geological Society of America Bulletin, 97:896-905; Doi: 10.1130/0016-7606(1986)97<896:Eotfte>2.0.Co;2

Craddock RA, Howard AD, Irwin RP, Tooth S, Williams RME, Chu P-S (2012) Drainage network development in the Keanakākoʻi tephra, Kīlauea Volcano, Hawaiʻi: Implications for fluvial erosion and valley network formation on early Mars. Journal of Geophysical Research, 117; Doi: 10.1029/2012je004074

Crosta GB, Dal Negro P (2003) Observations and modelling of soil slip-debris flow initiation processes in pyroclastic deposits: the Sarno 1998 event. Natural Hazards and Earth System Sciences, 3:53-69; Doi: 10.5194/nhess-3-53-2003

Cummans J (1980) Mudflows Resulting from the May 18, 1980, Eruption of Mount St. Helens, Washington. Geological Survey Circular, 850-B;

de Bélizal E, Lavigne F, Hadmoko DS, Degeai J-P, Dipayana GA, Mutaqin BW, Marfai MA, Coquet M, Mauff BL, Robin A-K, Vidal C, Cholik N, Aisyah N (2013) Rain-triggered lahars following the 2010 eruption of Merapi volcano, Indonesia: A major risk. Journal of Volcanology and Geothermal Research, 261:330-347; Doi: 10.1016/j.jvolgeores.2013.01.010

Donovan A, Eiser J, Sparks R (2014) Scientists' views about lay perceptions of volcanic hazard and risk. Journal of Applied Volcanology, 3:15; 10.1186/s13617-014-0015-5

Douillet GA, Pacheco DA, Kueppers U, Letort J, Tsang-Hin-Sun E, Bustillos J, Hall M, Ramon P, Dingwell DB (2013a) Dune bedforms produced by dilute pyroclastic density currents from the August 2006 eruption of Tungurahua volcano, Ecuador. Bulletin of Volcanology, 75; Doi: 10.1007/S00445-013-0762-X

Douillet GA, Tsang-Hin-Sun E, Kueppers U, Letort J, Pacheco DA, Goldstein F, Von Aulock F, Lavallee Y, Hanson JB, Bustillos J, Robin C, Ramon P, Hall M, Dingwell DB (2013b) Sedimentology and geomorphology of the deposits from the August 2006 pyroclastic density currents at Tungurahua volcano, Ecuador. Bulletin of Volcanology, 75; Doi: 10.1007/S00445-013-0765-7

Doyle E, Cronin S, Cole S, Thouret J (2009) The Challenges of Incorperating Temporal and Spatial Changes into Numerical Models of Lahars. Paper presented at the 18th World IMACS Congress and MODSIM09 International Congress on Modelling and Simulation,

Doyle EE, Cronin SJ, Cole SE, Thouret JC (2010) The coalescence and organization of lahars at Semeru volcano, Indonesia. Bulletin of Volcanology, 72:961-970; Doi: 10.1007/s00445-010-0381-8

Druzdzel MJ, van der Gaag LC (2000) Building probabilistic networks: "Where do the numbers come from?" guest editors' introduction. IEEE Transactions on Knowledge and Data Engineering, 12:481-486; Doi: 10.1109/tkde.2000.868901

Dumaisnil C, Thouret JC, Chambon G, Doyle EE, Cronin SJ, Surono (2010) Hydraulic, physical and rheological characteristics of rain-triggered lahars at Semeru volcano, Indonesia. Earth Surface Processes and landforms, 35:1573-1590; Doi: 10.1002/Esp.2003

Eychenne J, Le Pennec JL, Troncoso L, Gouhier M, Nedelec JM (2012) Causes and consequences of bimodal grain-size distribution of tephra fall deposited during the August 2006 Tungurahua eruption (Ecuador). Bulletin of Volcanology, 74:187-205; Doi: 10.1007/s00445-011-0517-5

Fagents SA, Baloga SM (2006) Toward a model for the bulking and debulking of lahars. J Geophys Res-Sol Ea, 111; Doi: 10.1029/2005jb003986

Fawcett T (2006) An introduction to ROC analysis. Pattern Recognition Letters, 27:861-874; Doi: 10.1016/j.patrec.2005.10.010

Fiksdal A (1982) Infiltration Rates of Undisturbed and Disturbed Mount St. Helens tephra deposits. Keller, S.A.C., ed. Mount St. Helens - One Year Later. Eastern Washington University Press, Cheney, WA

Folsom M (1986) Mount St. Helens tephra on range and forest lands of Eastern Washington-local erosion and redeposition. In: Keller, S.A.C., ed. Mount St. Helens-Five Years Later. Eastern Washington University Press, Cheney, WA

Garreaud RD (2009) The Andes climate and weather. Advances in Geosciences, 22:3-11; Doi: 10.5194/adgeo-22-3-2009

Gómez JA, Darboux F, Nearing MA (2003) Development and evolution of rill networks under simulated rainfall. Water Resources Research, 39; Doi: 10.1029/2002wr001437

Hall M, Robin C, Beate B, Mothes P, Monzier M (1999) Tungurahua Volcano, Ecuador: structure, eruptive history and hazards. Journal of Volcanology and Geothermal Research, 91:1-21; Doi: 10.1016/S0377-0273(99)00047-5

Hall ML, Steele AL, Mothes PA, Ruiz MC (2013) Pyroclastic density currents (PDC) of the 16–17 August 2006 eruptions of Tungurahua volcano, Ecuador: Geophysical registry and characteristics. Journal of Volcanology and Geothermal Research, 265:78-93; Doi: 10.1016/j.jvolgeores.2013.08.011

Hikida M, Moriyama M, Nagai Y (2007) Warning system for debris flow hazards at Sakurajima Volcano, Japan. Debris-Flow Hazards Mitigation: Mechanics, Prediction, and Assessment. Millpress Science Publishers, Rotterdam

Hodgson KA, Manville VR (1999) Sedimentology and flow behavior of a rain-triggered lahar, Mangatoetoenui Stream, Ruapehu volcano, New Zealand. Geological Society of America Bulletin, 111:743-754; Doi: 10.1130/0016-7606(1999)111<0743:safboa>2.3.co;2

Horton RE (1945) Erosional Development of Streams and Their Drainage Basins; Hydrophysical Approach to Quantitative Morphology. Geological Society of America Bulletin, 56:275; Doi: 10.1130/0016-7606(1945)56[275:edosat]2.0.co;2

Huang CJ, Shieh CL, Yin HY (2004) Laboratory study of the underground sound generated by debris flows. J Geophys Res-Earth, 109; Doi: 10.1029/2003jf000048

Hunink JE, Immerzeel WW, Droogers P (2014) A High-resolution Precipitation 2-step mapping Procedure (HiP2P): Development and application to a tropical mountainous area. Remote Sensing of Environment, 140:179-188; Doi: 10.1016/j.rse.2013.08.036

Iverson RM, Lahusen RG (1989) Dynamic pore-pressure fluctuations in rapidly shearing granular materials. Science, 246:796-799; Doi: 10.1126/science.246.4931.796

Iverson RM, Reid ME, Logan M, LaHusen RG, Godt JW, Griswold JP (2010) Positive feedback and momentum growth during debris-flow entrainment of wet bed sediment. Nature Geoscience, 4:116-121; Doi: 10.1038/ngeo1040

Janda R, Daag A, Delos Reyes P, Newhall C, Pierson T, Punongbayan R, Rodolfo K, Solidum R, Umbal J (1996) Assessment and Response to Lahar Hazard around Mt Pinatubo, 1991 to 1993. In: Newhall C, Punongbayan R (eds) Fire and Mud, Eruptions and Lahars of Mt Pinatubo, Philippines. PHIVOLCS/University of Washington Press, Quezon City/Seattle, pp 107-139

Kean JW, Staley DM, Cannon SH (2011) In situ measurements of post-fire debris flows in southern California: Comparisons of the timing and magnitude of 24 debris-flow events with rainfall and soil moisture conditions. J Geophys Res-Earth, 116; Doi: 10.1029/2011jf002005

Kilgour G, Manville V, Della Pasqua F, Graettinger A, Hodgson KA, Jolly GE (2010) The 25 September 2007 eruption of Mount Ruapehu, New Zealand: Directed ballistics, surtseyan jets, and ice-slurry lahars. Journal of Volcanology and Geothermal Research, 191:1-14; Doi: 10.1016/j.jvolgeores.2009.10.015

Kumagai H, Palacios P, Maeda T, Castillo DB, Nakano M (2009) Seismic tracking of lahars using tremor signals. Journal of Volcanology and Geothermal Research, 183:112-121; Doi: 10.1016/j.jvolgeores.2009.03.010

Lavigne F, Suwa H (2004) Contrasts between debris flows, hyperconcentrated flows and stream flows at a channel of Mount Semeru, East Java, Indonesia. Geomorphology, 61:41-58; Doi: 10.1016/j.geomorph.2003.11.005

Lavigne F, Thouret JC (2003) Sediment transportation and deposition by rain-triggered lahars at Merapi Volcano, Central Java, Indonesia. Geomorphology, 49:45-69; Doi: 10.1016/S0169-555x(02)00160-5

Lavigne F, Thouret JC, Hadmoko D, Sukatja B (2007) Lahars in Java: Initiations, Dynamic, Hazard Assessment and Deposition Processes. Forum Geografi, 21:17-32;

Lavigne F, Thouret JC, Voight B, Suwa H, Sumaryono A (2000a) Lahars at Merapi volcano, Central Java: an overview. Journal of Volcanology and Geothermal Research, 100:423-456; Doi: 10.1016/S0377-0273(00)00150-5

Lavigne F, Thouret JC, Voight B, Young K, LaHusen R, Marso J, Suwa H, Sumaryono A, Sayudi DS, Dejean M (2000b) Instrumental lahar monitoring at Merapi Volcano, Central Java, Indonesia. Journal of Volcanology and Geothermal Research, 100:457-478; Doi: 10.1016/S0377-0273(00)00151-7

Le Pennec J-L, Ruiz GA, Ramón P, Palacios E, Mothes P, Yepes H (2012) Impact of tephra falls on Andean communities: The influences of eruption size and weather conditions during the 1999–2001 activity of Tungurahua volcano, Ecuador. Journal of Volcanology and Geothermal Research, 217-218:91-103; Doi: 10.1016/j.jvolgeores.2011.06.011

Le Pennec JL, Jaya D, Samaniego P, Ramón P, Moreno Yánez S, Egred J, van der Plicht J (2008) The AD 1300–1700 eruptive periods at Tungurahua volcano, Ecuador, revealed by historical narratives, stratigraphy and radiocarbon dating. Journal of Volcanology and Geothermal Research, 176:70-81; Doi: 10.1016/j.jvolgeores.2008.05.019

Leavesley G, Lusby G, Lichty R (1989) Infiltration and Erosion Characteristics of Selected Tephra Deposits from the 1980 Eruption of Mt St Helens, Washington, USA. Hydrological Sciences, 34:339-353;

Lowe DR, Williams SN, Leigh H, Connort CB, Gemmell JB, Stoiber RE (1986) Lahars initiated by the 13 November 1985 eruption of Nevado del Ruiz, Colombia. Nature, 324:51-53; Doi: 10.1038/324051a0

Major J, Janda R, Daag A (1996) Watershed Disturbance and Lahars on the East Side of Mount Pinatubo during the Mid-June 1991 Eruptions. In: Newhall C, Punongbayan R (eds) Fire and Mud, Eruptions and Lahars of Mt Pinatubo, Philippines. PHIVOLCS/University of Washington Press, Quezon City/Seattle, pp 895-921

Major J, Yamakoshi T (2005) Decadal-scale change of infiltration characteristics of a tephra-mantled hillslope at Mount St Helens, Washington. Hydrological Processes, 19:3621-3630; Doi: 10.1002/Hyp.5863

Major JJ, Newhall CG (1989) Snow and ice perturbation during historical volcanic eruptions and the formation of lahars and floods. Bulletin of Volcanology, 52:1-27; Doi: 10.1007/bf00641384

Manville V, Cronin SJ (2007) Breakout Lahar From New Zealand's Crater Lake. Eos, Transactions American Geophysical Union, 88:441; Doi: 10.1029/2007eo430001

Manville V, Hodgson K, Houghton B, Keys J, White J (2000) Tephra, snow and water: complex sedimentary responses at an active snow-capped stratovolcano, Ruapehu, New Zealand. Bulletin of Volcanology, 62:278-293; Doi: 10.1007/s004450000096

Marchi L, Arattano M, Deganutti AM (2002) Ten years of debris-flow monitoring in the Moscardo Torrent (Italian Alps). Geomorphology, 46:1-17; Doi: 10.1016/S0169-555x(01)00162-3

Marcial S, Melosantos A, Hadley K, LaHusen R, Marso J (1996) Instrumental Lahar Monitoring at Mount Pinatubo. In: Newhall C, Punongbayan R (eds) Fire and Mud, Eruptions and Lahars of Mt Pinatubo, Philippines. PHIVOLCS/University of Washington Press, Quezon City/Seattle, pp 1015-1023

Martinez M, Arboleda R, Delos Reyes P, Gabinete E, Dolan M (1996) Observations of 1992 Lahars along the Sacobia-Bamban River System. In: Newhall C, Punongbayan R (eds) Fire and Mud, Eruptions and Lahars of Mt Pinatubo, Philippines. PHIVOLCS/University of Washington Press, Quezon City/Seattle, pp 1033-1045

Massey CI, Manville V, Hancox GH, Keys HJ, Lawrence C, McSaveney M (2009) Out-burst flood (lahar) triggered by retrogressive landsliding, 18 March 2007 at Mt Ruapehu, New Zealand—a successful early warning. Landslides, 7:303-315; Doi: 10.1007/s10346-009-0180-5

Murata KJ, Dondoli C, Saenz R (1966) The 1963–65 eruption of Irazú volcano, Costa Rica (the period of March 1963 to October 1964). Bulletin Volcanologique, 29:763-793; Doi: 10.1007/bf02597194

Myers ML, Geist DJ, Rowe MC, Harpp KS, Wallace PJ, Dufek J (2014) Replenishment of volatile-rich mafic magma into a degassed chamber drives mixing and eruption of Tungurahua volcano. Bulletin of Volcanology, 76; Doi: 10.1007/S00445-014-0872-0

Ogawa Y, Daimaru H, Shimizu A (2007) Experimental study of post-eruption overland flow and sediment load from slopes overlain by pyroclastic-flow deposits, Unzen volcano, Japan. Geomorphologie:237-246;

Okano K, Suwa H, Kanno T (2012) Characterization of debris flows by rainstorm condition at a torrent on the Mount Yakedake volcano, Japan. Geomorphology, 136:88-94; Doi: 10.1016/j.geomorph.2011.04.006

Pierson T, Daag A, Delos Reyes P, TM R, Solidum R, Tubianosa B (1996) Flow and Deposition of Posteruption Hot Lahars on the East Side of Mount Pinatubo, July-October 1991. In: Newhall C, Punongbayan R (eds) Fire and Mud, Eruptions and Lahars of Mt Pinatubo, Philippines. PHIVOLCS/University of Washington Press, Quezon City/Seattle, pp 921-951

Pierson TC, Janda RJ, Thouret J-C, Borrero CA (1990) Perturbation and melting of snow and ice by the 13 November 1985 eruption of Nevado del Ruiz, Colombia, and consequent mobilization, flow and deposition of lahars. Journal of Volcanology and Geothermal Research, 41:17-66; Doi: 10.1016/0377-0273(90)90082-q

Reid M, Iverson R, Logan M, Lahusen RG, Godt J, Griswold J (2011) Entrainment of Bed Sediment By Debris Flows: Results From Large Scale Experiments. Paper presented at the Fifth International Conference on Debris-flow Hazards Mitigation, Mechanics, Prediction and Assessment, Casa Editrice Universita La Sapienza, Rome,

Rodolfo K, Arguden A (1991) Rain-Lahar Generation and Sediment-Delivery systems at Mayon Volcano, Philippines. In: RV F, GA S (eds) Sedimentation in Volcanic Settings, vol 45. Society of Economic Paleontologists and Mineralogists, Special Publications, pp 71-88

Rodolfo K, Umbal J, Alonso R, Remotigue C, Paladio-Melosantos L, Salvador J, Evangelista D, Miller Y (1996) Two Years of Lahars on the Western Flank of Mount Pinatubo: Initiation, Flow Processes, Deposits, and Attendant Geomorphic and Hydraulic Changes. In: Newhall C, Punongbayan R (eds) Fire and Mud, Eruptions and Lahars of Mt Pinatubo, Philippines. PHIVOLCS/University of Washington Press, Quezon City/Seattle, pp 989-1015

Samaniego P, Le Pennec JL, Robin C, Hidalgo S (2011) Petrological analysis of the pre-eruptive magmatic process prior to the 2006 explosive eruptions at Tungurahua volcano (Ecuador). Journal of Volcanology and Geothermal Research, 199:69-84; Doi: 10.1016/j.jvolgeores.2010.10.010

Schneider D, Bartelt P, Caplan-Auerbach J, Christen M, Huggel C, McArdell BW (2010) Insights into rock-ice avalanche dynamics by combined analysis of seismic recordings and a numerical avalanche model. J Geophys Res-Earth, 115; Doi: 10.1029/2010jf001734

Scott K, Janda R, De La Cruz E, Gabinete E, Eto I, Isada M, Sexon M, Hadley K (1996) Channel and Sedimentation Responses to Large Volumes of 1991 Volcanic Deposits on the East Flank of Mt Pinatubo. In: Newhall C, Punongbayan R (eds) Fire and Mud, Eruptions and Lahars of Mt Pinatubo, Philippines. PHIVOLCS/University of Washington Press, Quezon City/Seattle, pp 971-989

Smith GA, Fritz WJ (1989) Volcanic Influences on Terrestrial Sedimentation. Geology, 17:375-376;

Sorenson O, Rose W, Jaya D (2003) Lahar Hazard Modelling at Tungurahua, Ecuador. Paper presented at the GS - AGU - EUG Joint Assembly, Nice, France,

Stone J, Barclay J, Simmons P, Cole PD, Loughlin SC, Ramón P, Mothes P (2014) Risk reduction through community-based monitoring: the vigías of Tungurahua, Ecuador. Journal of Applied Volcanology, 3:11; Doi: 10.1186/s13617-014-0011-9

Swets J, Dawes R, Monahan J (1988) Better Decisions through Science. Scientific American, 240:1285-1293;

Todisco F (2014) The internal structure of erosive and non-erosive storm events for interpretation of erosive processes and rainfall simulation. Journal of Hydrology, 519:3651-3663; Doi: 10.1016/j.jhydrol.2014.11.002

Tungol N, Regalado T (1996) Rainfall, Acoustic Flow Monitor Records, and Observed Lahars of the Sacobia River in 1992. In: Newhall C, Punongbayan R (eds) Fire and Mud, Eruptions and Lahars of Mt Pinatubo, Philippines. PHIVOLCS/University of Washington Press, Quezon City/Seattle, pp 1023-1033

Van Westen C, Daag A (2005) Analysing the Relation Between Rainfall Characteristics and Lahar Activity at Mt Pinatubo, Philippines. Earth Surface Processes and Landforms, 30:1663-1674;

Waldron H (1967) Debris Flow and Erosion Control problems caused by the Ash eruptions of Irazu. Contributions to General Geology - 1966, 1241-1;

Wang L, Shi ZH, Wang J, Fang NF, Wu GL, Zhang HY (2014) Rainfall kinetic energy controlling erosion processes and sediment sorting on steep hillslopes: A case study of clay loam soil from the Loess Plateau, China. Journal of Hydrology, 512:168-176; Doi: 10.1016/j.jhydrol.2014.02.066

Waythomas CF, Pierson TC, Major JJ, Scott WE (2013) Voluminous ice-rich and water-rich lahars generated during the 2009 eruption of Redoubt Volcano, Alaska. Journal of Volcanology and Geothermal Research, 259:389-413; Doi: 10.1016/j.jvolgeores.2012.05.012

Williams R, Stinton AJ, Sheridan MF (2008) Evaluation of the Titan2D two-phase flow model using an actual event: Case study of the 2005 Vazcun Valley Lahar. Journal of Volcanology and Geothermal Research, 177:760-766; Doi: 10.1016/j.jvolgeores.2008.01.045

Wischmeier W, Smith D (1978) Prediciting rainfall erosion losses - A guide to conservation planning. Agricultural Handbooks (USA) No. 537. US Department of Agriculture, Washington DC

Yamakoshi T, Suwa H (2000) Post-Eruption Characteristics of Surface Runoff and Sediment Discharge on the Slopes of Pyroclastic-Flow Deposits, Mt Unzen, Japan. Transactions, Japanese Geomorphological Union, 21:469-497;

Zanchetta G, Sulpizio R, Pareschi MT, Leoni FM, Santacroce R (2004) Characteristics of May 5–6, 1998 volcaniclastic debris flows in the Sarno area (Campania, southern Italy):

relationships to structural damage and hazard zonation. Journal of Volcanology and Geothermal Research, 133:377-393; Doi: 10.1016/s0377-0273(03)00409-8

Zobin VM, Plascencia I, Reyes G, Navarro C (2009) The characteristics of seismic signals produced by lahars and pyroclastic flows: Volcán de Colima, México. Journal of Volcanology and Geothermal Research, 179:157-167; Doi: 10.1016/j.jvolgeores.2008.11.001

Figure Captions:

Fig. 1 Location Map of Tungurahua Volcano.

Fig. 2 (A) Early Stages of the 12th February 2005 Vazcun Valley lahar. Flow front is visible at the upstream end of the El Salado Baths. (B) Peak stage height of the 12th February 2005 Vazcun Valley lahar. (C) Efforts to clear the Baños to Pan-American Highway link in October 2007 after a lahar in the La Pampa drainage inundated the road. All photos courtesy of IGEPN.

Fig. 3 Shaded relief DEM map of the northern slopes of Tungurahua Volcano. The catchment upstream of the La Pampa AFM is displayed in green and the catchment upstream of the Vazcun AFM is displayed in red.

Fig. 4 Lahar alert triggering rainfall intensity vs duration plot for Vazcun and La Pampa lahar alerts between March 2012 and June 2013. Upper and lower power-law best fit curves illustrate the boundaries of the estimated lahar alert triggering zone. Lower boundary curves for Mayon volcano debris flows between 1986 and 1989 (Rodolfo and Arguden 1991); Pinatubo Pasig-Potrero lahars in 1992 (Arboleda and Martinez 1996) and Pinatubo Sacobia lahars in 1992 (Tungol and Regalado 1996) are also displayed for comparison.

Fig. 5 Timeline displaying the elapsed time since the last reported PDC activity at Tungurahua (dashed line), the number of daily recorded daily explosions (green) and the daily rainfall (blue) between 1st February 2012 and 20th June 2013. The occurrence of lahar alert signals (red) is also depicted.

Fig. 6 (A), (B) and (C) show Receiver Operating Characteristic (ROC) curves displaying the ability of several variables to predict the occurrence of lahar alerts. The diagonal reference lines are an example of an idealised random relationship. The accompanying table (D) describes the output statistics relating to the lahar alert centric ROC curves.

Fig. 7 Two-Dimensional probability plots displaying the variation in lahar alert probability as peak rainfall intensity increases. 10 minute peak rainfall intensity (top); 30 minute peak rainfall intensity (middle); 1 hour peak rainfall intensity (bottom). March 2012-December 2013 data.

Fig. 8 Three dimensional probability plots depicting the probability of a lahar alert (scale on vertical axis) in the Vazcun and La Pampa drainages based on various peak rainfall intensities and antecedent rainfall conditions. March 2012-December 2013.

Fig. 9 Lahar Alert event which occurred on December 20th 2013. 3 of the 12 lahar alert probability matrices shown in fig. 8 are utilised in conjunction with “real-time” rainfall data to produce dynamic lahar alert occurrence probabilities throughout the rainfall event.

Fig.10 Receiver Operating Characteristic (ROC) curves describing the ability of several of the probability matrices shown in table 1 to predict the generation of lahar alert signals between July and December 2013. Corresponding ROC curve areas are displayed in the figure legend. The diagonal reference line depicts an example of a random relationship.

Table Captions:

Table 1 Peak estimated lahar alert probabilities during all ≥10 mm rainfall events occurring between July 1^{st} and December 31^{st} 2013; as predicted by all available probability matrices. In addition to the outputs of the individual probability matrices (columns A-O), categorised mean probabilities are also displayed (columns P-Y). Black rows depict lahar alert producing events. Grey rows represent events which did not trigger a lahar alert signal. White rows display events which did not feature available AFM data.

Table 2 Summary statistics relating to the Receiver Operating Characteristic (ROC) analysis of the probability estimates shown in *table 1,* with respect to their ability to effectively predict lahar alert signals between 1^{st} July and 31^{st} December 2013. Grey rows indicate the matrices shown in *Fig. 9.*

Table 3 Analysis of the additional warning time that is provided by the various probability matrices when applied to the eight lahar alert signal producing events between 1^{st} July and 31^{st} December 2013. The time-scale of the antecedent rainfall consideration is not considered in this table as it only impacts the magnitude of the peak probability and has no effect upon its timing.

Figure1: Broad Location Map
Click here to download Figure: fig1.tif

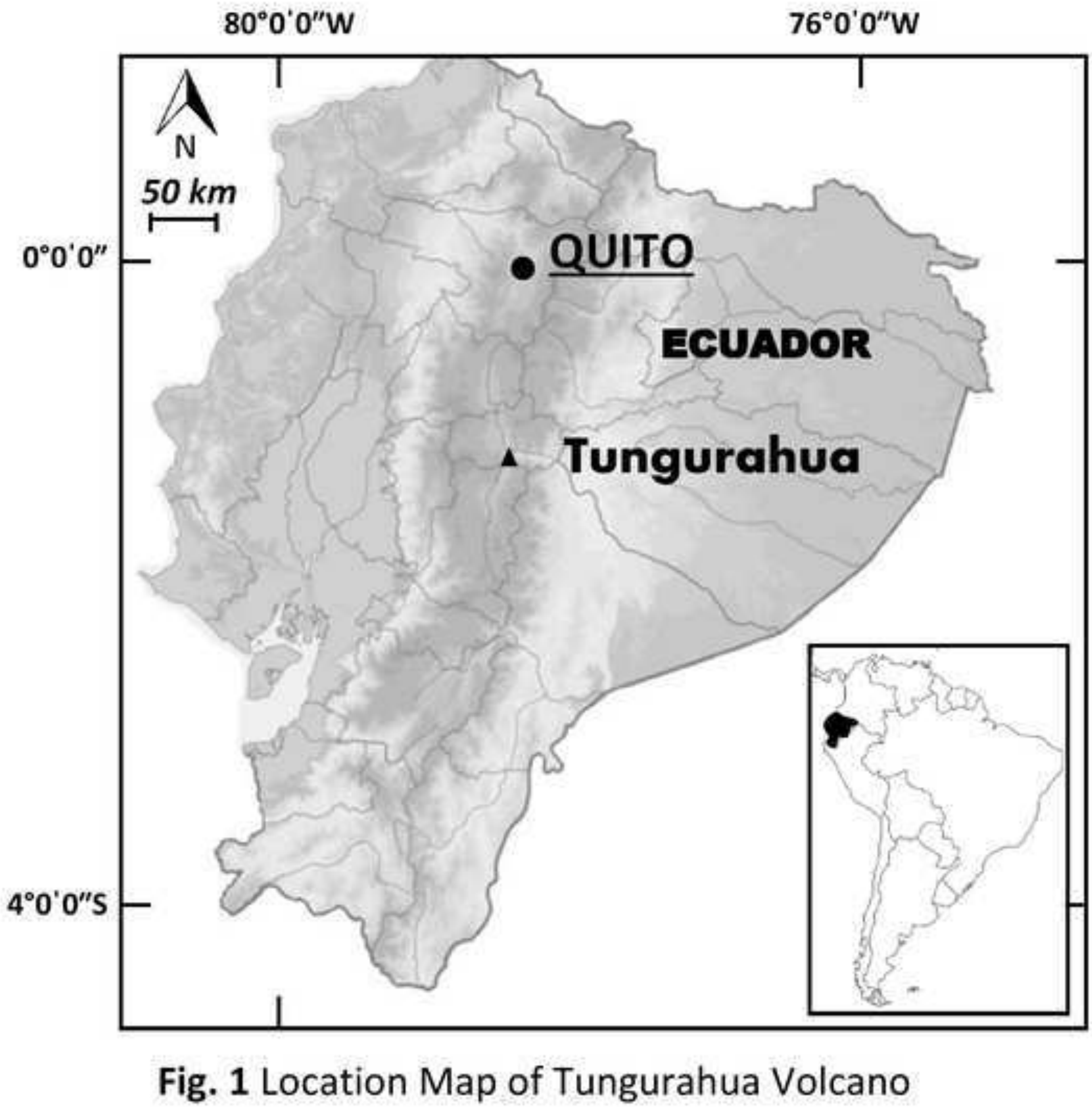

Fig. 1 Location Map of Tungurahua Volcano

Figure 2: Tungurahua Lahar Photos
Click here to download Figure: Fig2.tif

Fig. 2 (A) Early Stages of the 12^{th} February 2005 Vazcun Valley lahar. Flow front is visible at the upstream end of the El Salado Baths. (B) Peak stage height of the 12^{th} February 2005 Vazcun Valley lahar. (C) Efforts to clear the Baños to Pan-American Highway link in October 2007 after a lahar in the La Pampa drainage inundated the road. All photos courtesy of IGEPN

Figure 3: Specific Location Map
Click here to download Figure: Fig3.tif

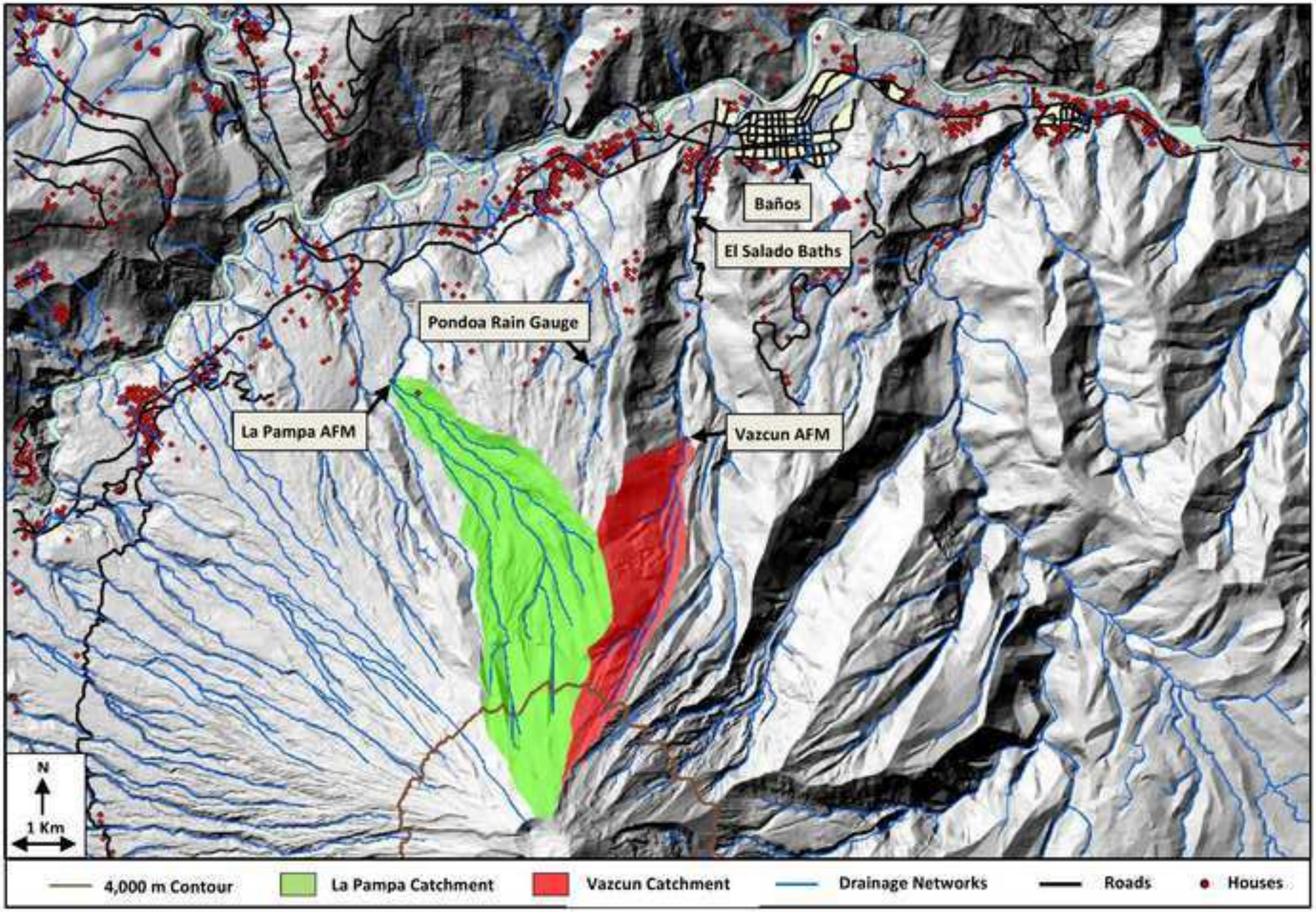

Fig. 3 Shaded relief DEM map of the northern slopes of Tungurahua Volcano. The catchment upstream of the La Pampa AFM is displayed in green and the catchment upstream of the Vazcun AFM is displayed in red

Figure 4: Intensity/Duration Analysis
Click here to download Figure: Fig4.tif

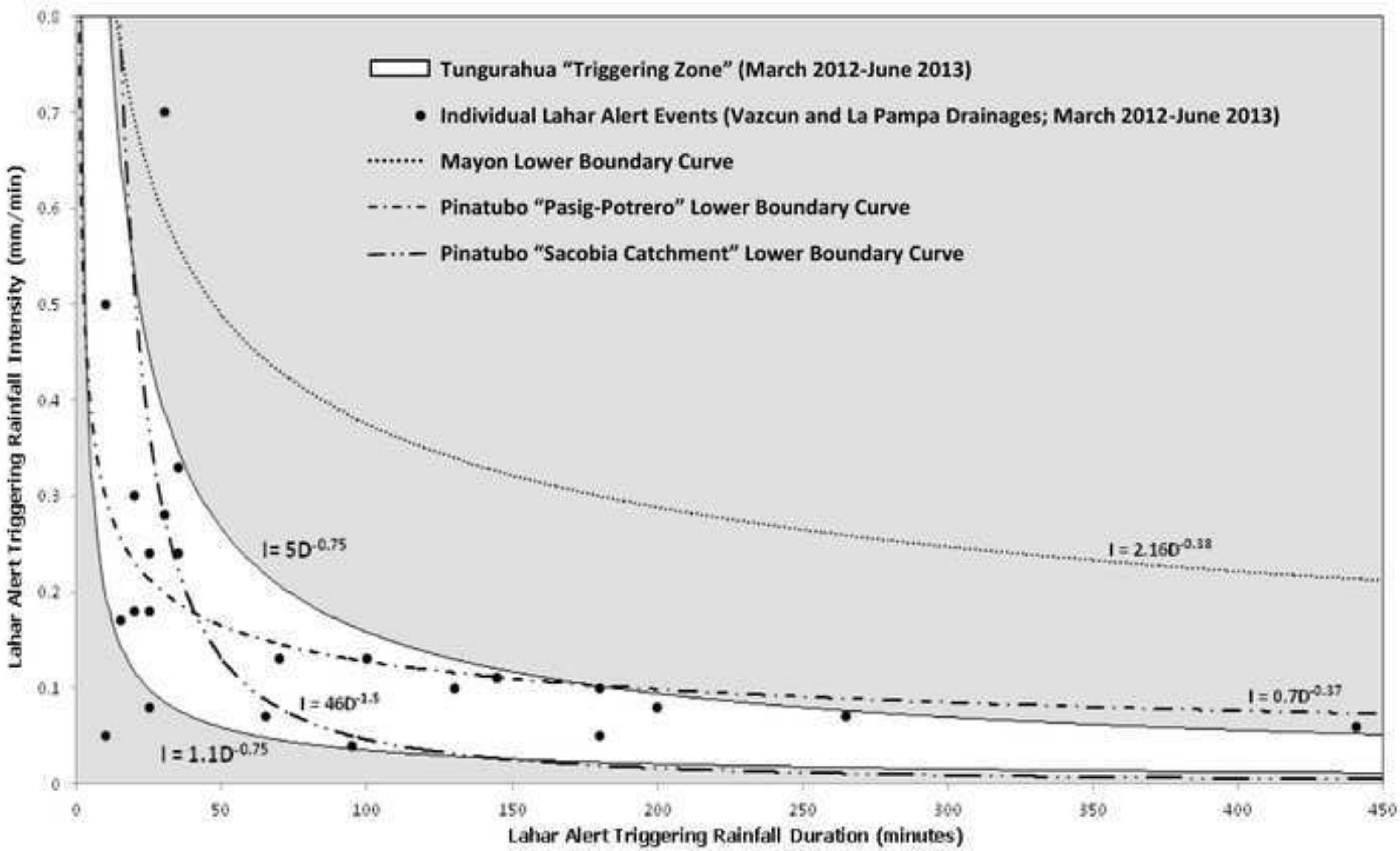

Fig. 4 Lahar alert triggering rainfall intensity vs duration plot for Vazcun and La Pampa lahar alerts between March 2012 and June 2013. Upper and lower power-law best fit curves illustrate the boundaries of the estimated lahar alert triggering zone. Lower boundary curves for Mayon volcano debris flows between 1986 and 1989 *(Rodolfo and Arguden, 1991)*; Pinatubo Pasig-Potrero lahars in 1992 *(Arboleda and Martinez, 1996)* and Pinatubo Sacobia lahars in 1992 *(Tungol and Regalado, 1996)* are also displayed

Figure 5: Tungurahua Timeline

Click here to download Figure: fig5.tif

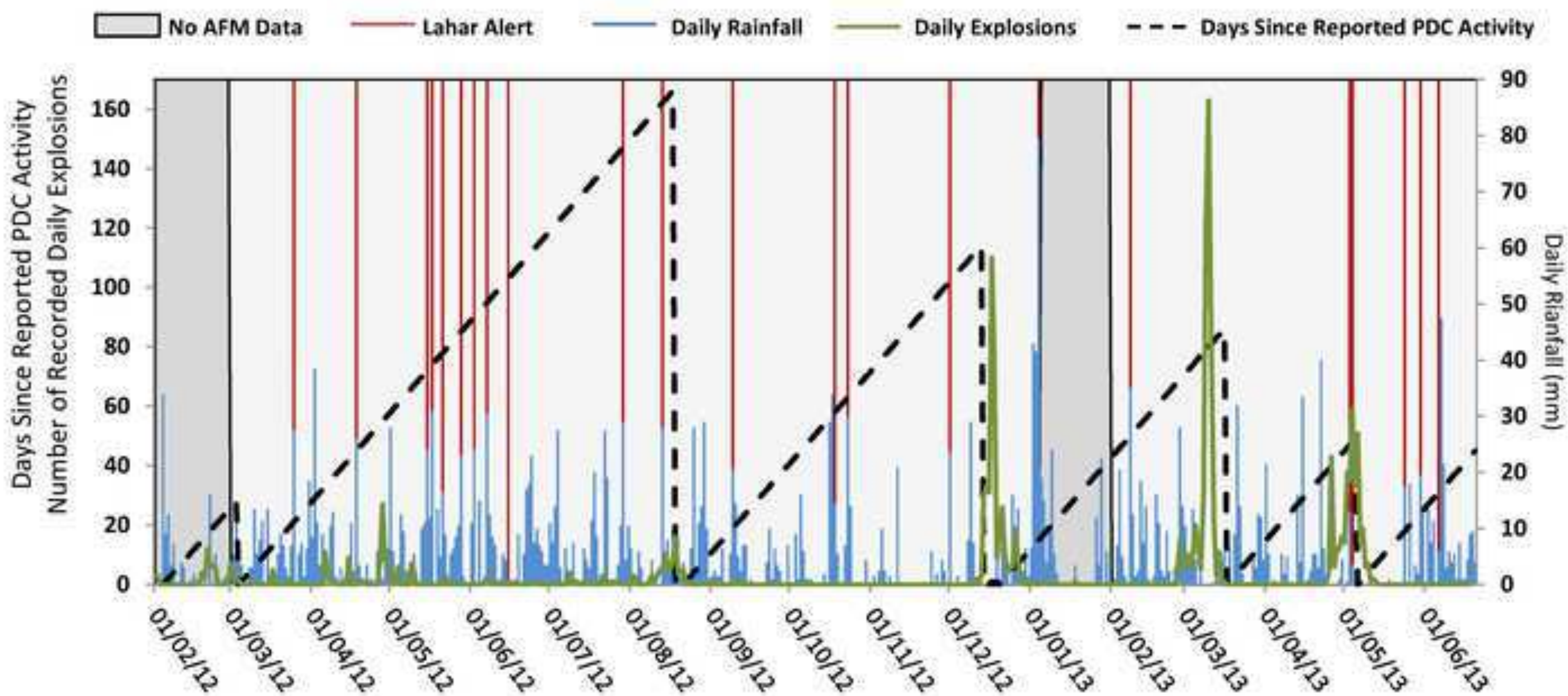

Fig. 5 Timeline displaying the elapsed time since the last reported PDC activity at Tungurahua (dashed line), the number of daily recorded daily explosions (green) and the daily rainfall (blue) between 1st February 2012 and 20th June 2013. The occurrence of lahar alert signals (red) is also depicted

Figure 6: ROC Curves

Click here to download Figure: Fig6.tif

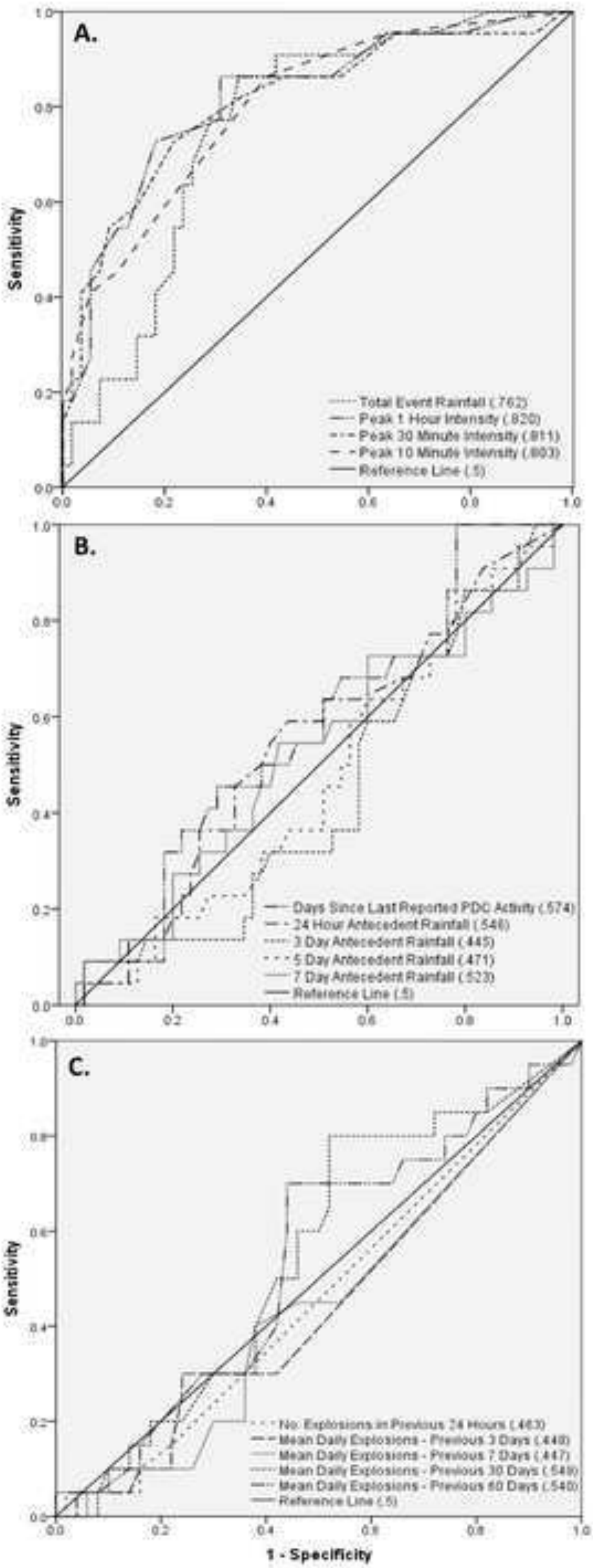

D. Area Under the Curve Statistics

Test Result Variable(s)	Area	Standard Error[a]	*P*-Value[b]
Total Event Rainfall	.762	.056	.000
Peak 1 Hour Rainfall Intensity	.820	.055	.000
Peak 30 Minute Rainfall Intensity	.811	.058	.000
Peak 10 Minute Rainfall Intensity	.803	.055	.000
Time Since Last PDC Activity	.574	.070	.316
24 Hour Antecedent Rainfall	.546	.072	.531
3 Day Antecedent Rainfall	.445	.071	.450
5 Day Antecedent Rainfall	.471	.071	.689
7 Day Antecedent Rainfall	.523	.075	.752
Mean Daily Explosions – Previous 24 Hours	.463	.075	.631
Mean Daily Explosions – Previous 3 Days	.448	.076	.495
Mean Daily Explosions – Previous 7 Days	.447	.075	.487
Mean Daily Explosions – Previous 30 Days	.549	.073	.528
Mean Daily Explosions – Previous 60 Days	.540	.075	.603

a. Under the nonparametric assumption
b. Null hypothesis: true area = 0.5.

Fig. 6 (A), (B) and (C) show Receiver Operating Characteristic (ROC) curves displaying the ability of several variables to predict the occurrence of lahar alerts. The diagonal reference lines are an example of an idealised random relationship. The accompanying table (D) describes the output statistics relating to the lahar alert centric ROC curves

Figure 7: 2D Probability Plots

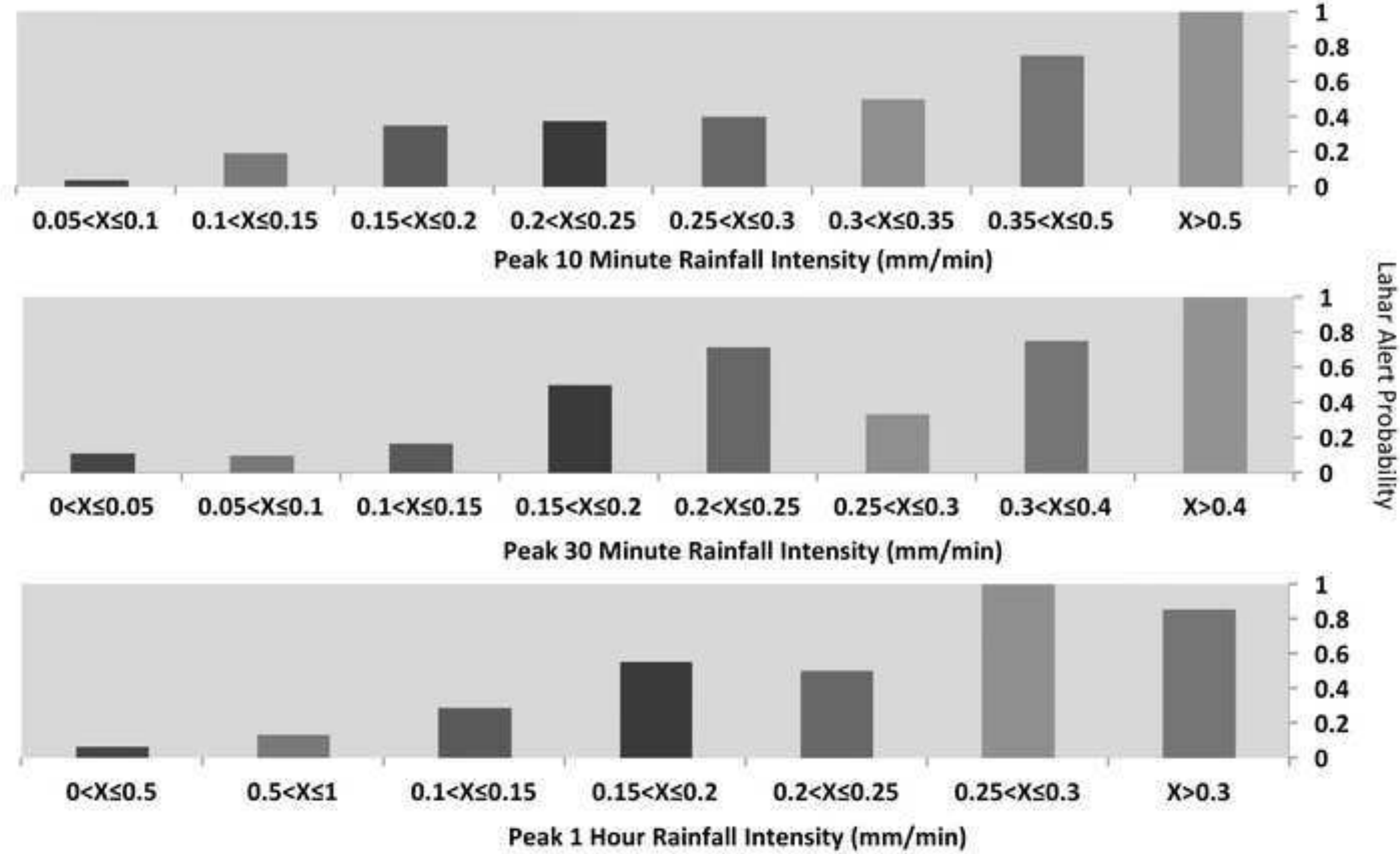

Fig. 7 Two-Dimensional probability plots displaying the variation in lahar alert probability as peak rainfall intensity increases. 10 minute peak rainfall intensity (top); 30 minute peak rainfall intensity (middle); 1 hour peak rainfall intensity (bottom). March 2012-December 2013 data

Figure 8: 3D Probability Plots
Click here to download Figure: fig8.tif

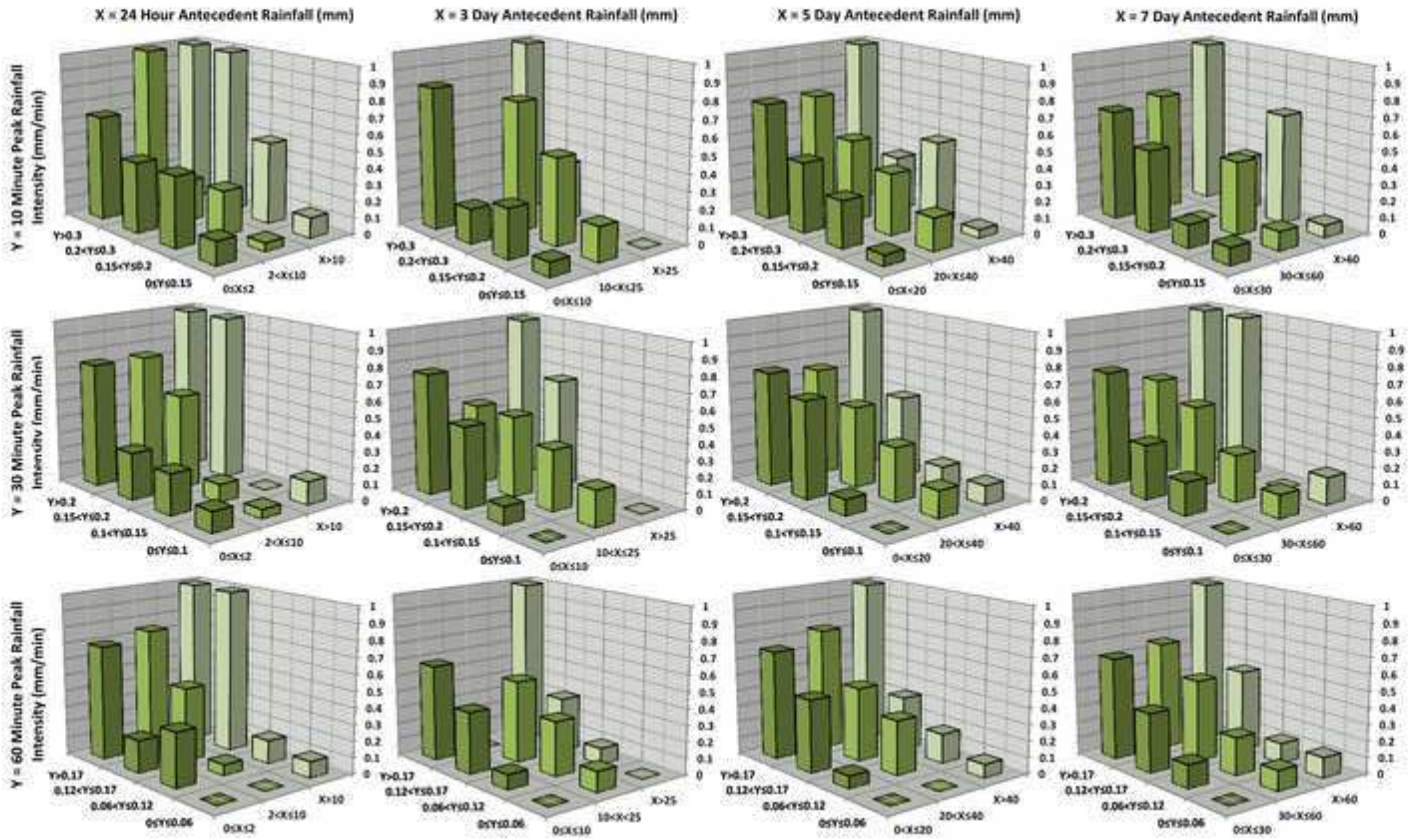

Fig. 8 Three dimensional probability plots depicting the probability of a lahar alert (scale on vertical axis) in the Vazcun and La Pampa drainages based on various peak rainfall intensities and antecedent rainfall conditions. March 2012-December 2013

Figure 9: Single Event
Click here to download Figure: Fig9.tif

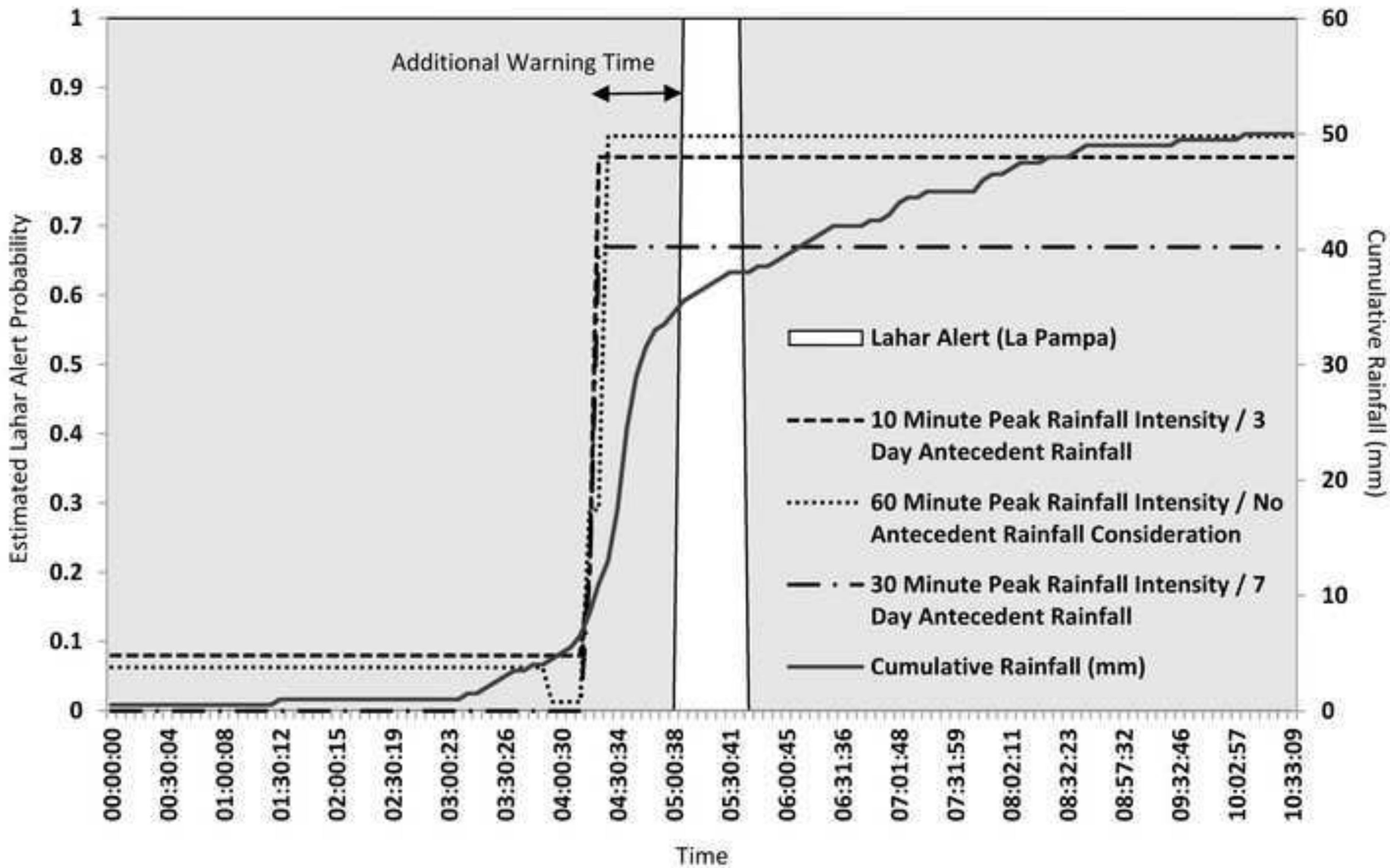

Fig. 9 Lahar Alert event which occurred on December 20th 2013. 3 of the 12 lahar alert probability matrices shown in *fig. 8* are utilised in conjunction with "real-time" rainfall data to produce dynamic lahar alert occurrence probabilities throughout the rainfall event

Figure 10: Selected ROC Curves
Click here to download Figure: Fig10.tif

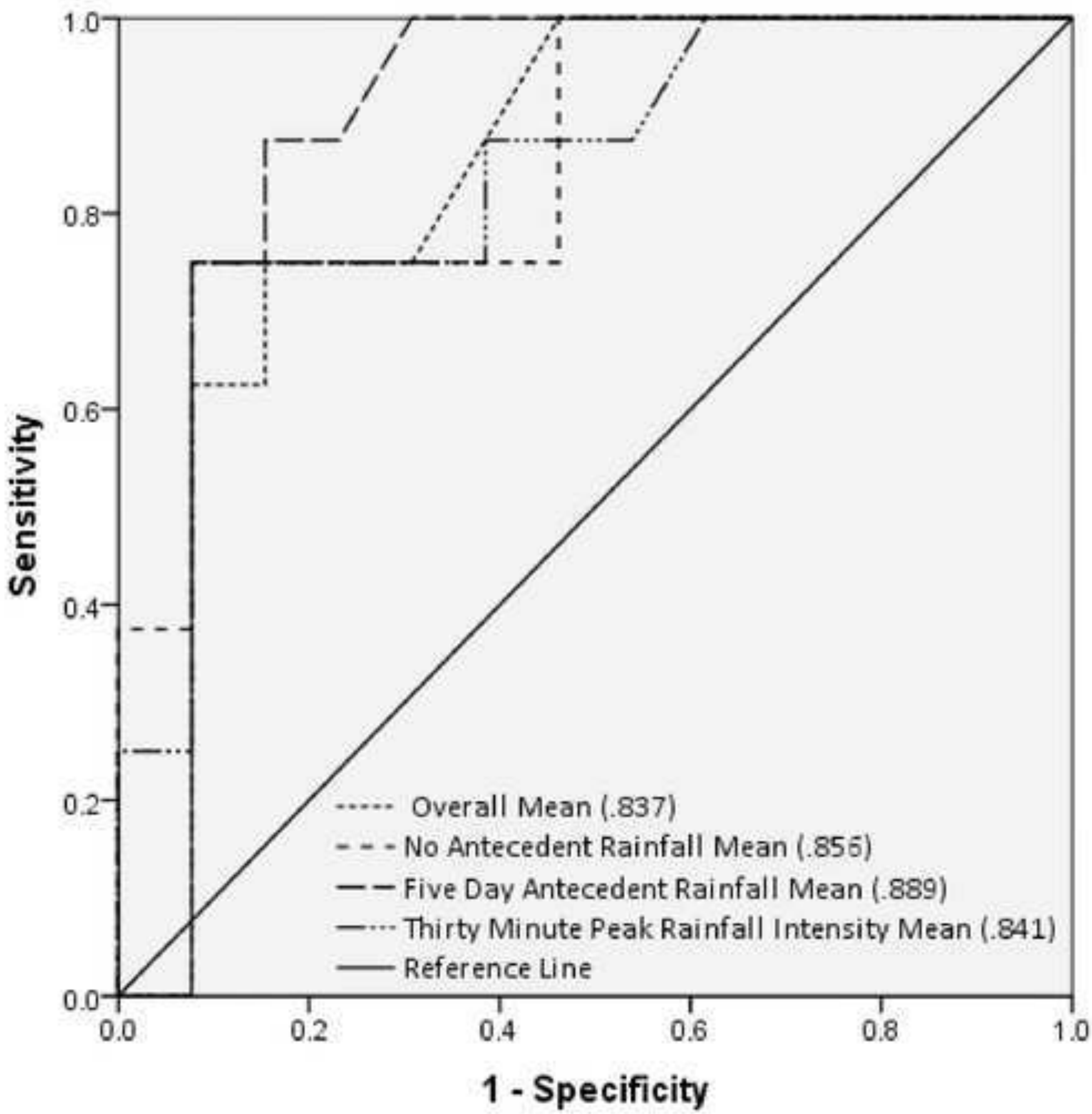

Fig.10 Receiver Operating Characteristic (ROC) curves describing the ability of several of the probability matrices shown in table 1 to predict the generation of lahar alert signals between July and December 2013. Corresponding ROC curve areas are displayed in the figure legend. The diagonal reference line depicts an example of a random relationship

Table 1: Estimated Probability Table

Click here to download Table: Table1.tif

Table 1 Peak estimated lahar alert probabilities during all ≥10 mm rainfall events occurring between July 1st and December 31st 2013; as predicted by all available probability matrices. In addition to the outputs of the individual probability matrices (columns A-O), categorised mean probabilities are also displayed (columns P-Y). Black rows depict lahar alert producing events. Grey rows represent events which did not trigger a lahar alert signal. White rows display events which did not feature available AFM data

	A	B	C	D	E	F	G	H	I	J	K	L	M	N	O	P	Q	R	S	T	U	V	W	X	Y		
	No Antecedent Rainfall Consideration			24 Hour Antecedent Rainfall Consideration			3 Day Antecedent Rainfall Consideration			5 Day Antecedent Rainfall Consideration			7 Day Antecedent Rainfall Consideration														
Rainfall Event Start Date	10 Minute Peak Rainfall Intensity	30 Minute Peak Rainfall Intensity	60 Minute Peak Rainfall Intensity	10 Minute Peak Rainfall Intensity	30 Minute Peak Rainfall Intensity	60 Minute Peak Rainfall Intensity	10 Minute Peak Rainfall Intensity	30 Minute Peak Rainfall Intensity	60 Minute Peak Rainfall Intensity	10 Minute Peak Rainfall Intensity	30 Minute Peak Rainfall Intensity	60 Minute Peak Rainfall Intensity	10 Minute Peak Rainfall Intensity	30 Minute Peak Rainfall Intensity	60 Minute Peak Rainfall Intensity	Overall Mean	"No Antecedent Rainfall" Mean	Antecedent Rainfall Mean (All Timescales)	24 Hour Antecedent Rainfall Mean	3 Day Antecedent Rainfall Mean	5 Day Antecedent Rainfall Mean	7 Day Antecedent Rainfall Mean	10 Minute Peak Rainfall Intensity Mean	30 Minute Peak Rainfall Intensity Mean	60 Minute Peak Rainfall Intensity Mean	Alert	Alert Extent
07/07/13	0.35	0.17	0.29	0.43	0.25	0.20	0.29	0.11	0.38	0.29	0.10	0.44	NA	NA	NA	0.28	0.27	0.28	0.29	0.26	0.28	NA	0.34	0.16	0.26	NA	NA
09/07/13	0.67	0.47	0.26	0.60	0.17	0.29	1.00	0.50	0.00	0.67	0.43	0.27	0.67	0.43	0.17	0.44	0.46	0.43	0.35	0.50	0.46	0.42	0.72	0.40	0.16	Yes	LP
12/07/13	0.04	0.10	0.14	0.06	0.06	0.00	0.21	0.24	0.14	0.06	0.13	0.09	0.13	0.15	0.14	0.11	0.09	0.12	0.04	0.20	0.09	0.14	0.10	0.14	0.08	No	NA
15/07/13	0.15	0.08	0.10	0.00	0.00	0.00	0.16	0.18	0.29	0.14	0.09	0.27	0.06	0.08	0.17	0.12	0.11	0.12	0.00	0.21	0.17	0.10	0.10	0.09	0.14	Yes	LP&V
24/07/13	0.19	0.17	0.29	0.05	0.11	0.07	0.08	0.11	0.09	0.07	0.10	0.08	0.11	0.20	0.14	0.12	0.22	0.10	0.08	0.09	0.08	0.15	0.10	0.14	0.11	NA	NA
29/07/13	0.19	0.10	0.13	0.05	0.06	0.07	0.08	0.00	0.09	0.05	0.12	0.18	0.12	0.14	0.23	0.11	0.14	0.10	0.06	0.06	0.12	0.16	0.10	0.08	0.12	NA	NA
02/08/13	0.40	0.71	0.56	0.25	0.75	0.75	0.33	1.00	1.00	0.33	1.00	1.00	0.33	1.00	1.00	0.69	0.56	0.73	0.58	0.78	0.78	0.78	0.33	0.89	0.72	NA	NA
06/08/13	0.19	0.10	0.13	0.05	0.06	0.07	0.00	0.00	0.10	0.05	0.12	0.18	0.08	0.17	0.13	0.10	0.14	0.08	0.06	0.03	0.12	0.12	0.07	0.09	0.10	NA	NA
13/08/13	0.19	0.17	0.13	0.05	0.11	0.07	0.08	0.11	0.09	0.07	0.10	0.08	0.11	0.20	0.14	0.11	0.16	0.10	0.08	0.09	0.08	0.15	0.10	0.14	0.08	NA	NA
14/08/13	0.04	0.10	0.13	0.13	0.14	0.10	0.20	0.22	0.13	0.20	0.17	0.00	0.12	0.14	0.13	0.13	0.09	0.14	0.32	0.18	0.12	0.13	0.14	0.15	0.08	NA	NA
16/08/13	0.19	0.17	0.13	0.14	0.25	0.33	0.20	0.38	0.33	0.20	0.33	0.33	0.12	0.29	0.23	0.24	0.16	0.26	0.24	0.30	0.29	0.21	0.17	0.28	0.23	NA	NA
26/08/13	0.04	0.10	0.07	0.15	0.14	0.00	0.09	0.00	0.00	0.07	0.00	0.00	0.11	0.00	0.00	0.05	0.07	0.05	0.10	0.03	0.02	0.04	0.09	0.05	0.01	No	NA
28/08/13	0.04	0.10	0.07	0.15	0.14	0.00	0.21	0.24	0.14	0.07	0.00	0.00	0.11	0.00	0.00	0.08	0.07	0.09	0.10	0.20	0.02	0.04	0.12	0.10	0.03	No	NA
31/08/13	0.15	0.13	0.10	0.08	0.18	0.29	0.00	0.00	0.00	0.14	0.20	0.27	0.06	0.11	0.08	0.12	0.13	0.12	0.18	0.00	0.20	0.08	0.08	0.12	0.12	Yes	LP
09/09/13	0.20	0.10	0.14	0.06	0.06	0.07	0.21	0.24	0.36	0.07	0.00	0.08	0.11	0.00	0.15	0.12	0.13	0.12	0.06	0.27	0.05	0.09	0.13	0.08	0.13	No	NA
15/09/13	0.20	0.10	0.14	0.15	0.14	0.36	0.09	0.00	0.10	0.07	0.00	0.08	0.11	0.00	0.15	0.11	0.15	0.10	0.22	0.06	0.05	0.09	0.12	0.05	0.14	No	NA
17/09/13	0.25	0.67	0.50	0.33	0.72	0.11	0.67	0.33	0.45	0.00	0.60	0.40	0.43	0.67	0.30	0.43	0.47	0.42	0.39	0.48	0.33	0.47	0.34	0.60	0.29	Yes	LP
29/09/13	0.32	0.47	0.26	0.33	0.17	0.11	0.17	0.40	0.29	0.17	0.50	0.38	0.00	0.20	0.30	0.27	0.35	0.25	0.20	0.29	0.35	0.17	0.20	0.35	0.22	Yes	LP
04/10/13	0.20	0.10	0.14	0.05	0.06	0.07	0.21	0.24	0.36	0.07	0.00	0.08	0.13	0.15	0.25	0.14	0.15	0.14	0.06	0.27	0.05	0.18	0.13	0.11	0.15	No	NA
08/10/13	0.10	0.04	0.10	0.07	0.15	0.14	0.00	0.21	0.24	0.14	0.21	0.18	0.00	0.13	0.15	0.12	0.08	0.13	0.12	0.15	0.18	0.09	0.06	0.15	0.14	No	NA
14/10/13	0.37	0.17	0.30	0.30	0.13	0.07	0.56	0.43	0.36	0.33	0.11	0.08	0.50	0.33	0.25	0.29	0.28	0.29	0.17	0.45	0.17	0.36	0.41	0.23	0.18	No	NA
16/10/13	0.04	0.10	0.14	0.15	0.14	0.36	0.21	0.24	0.36	0.21	0.18	0.36	0.11	0.00	0.15	0.18	0.09	0.21	0.22	0.27	0.25	0.09	0.14	0.13	0.23	No	NA
22/10/13	0.04	0.10	0.14	0.15	0.14	0.36	0.09	0.00	0.10	0.07	0.00	0.08	0.11	0.00	0.15	0.10	0.09	0.10	0.22	0.06	0.05	0.09	0.09	0.05	0.14	No	NA
13/11/13	0.37	0.17	0.30	0.30	0.13	0.07	NA	NA	NA	NA	NA	NA	NA	NA	NA	0.22	0.28	0.17	0.17	NA	NA	NA	0.34	0.15	0.12	No	NA
17/11/13	1.00	0.67	1.00	0.60	0.73	0.67	0.80	0.73	0.55	0.67	0.60	0.67	NA	NA	NA	0.72	0.89	0.67	0.67	0.69	0.65	NA	0.77	0.68	0.58	Yes	LP&V
26/11/13	1.00	1.00	0.83	0.60	0.73	0.67	0.80	0.73	0.55	0.67	0.67	0.63	0.60	0.67	0.57	0.71	0.94	0.66	0.67	0.69	0.66	0.61	0.73	0.76	0.54	Yes	LP
30/11/13	0.60	0.50	0.65	0.70	0.82	0.78	0.90	0.82	0.64	0.83	0.80	1.00	0.63	0.75	1.00	0.77	0.58	0.82	0.77	0.79	0.88	0.86	0.77	0.74	0.68	No	NA
20/12/13	1.00	1.00	0.83	0.60	0.73	0.67	0.80	0.73	0.55	0.67	0.67	0.63	0.60	0.67	0.57	0.71	0.94	0.66	0.67	0.69	0.66	0.61	0.73	0.76	0.54	Yes	LP
27/12/13	0.20	0.10	0.14	0.06	0.06	0.07	0.09	0.00	0.10	0.07	0.00	0.08	0.11	0.00	0.15	0.08	0.15	0.07	0.06	0.06	0.05	0.09	0.11	0.03	0.09	No	NA
28/12/13	0.04	0.10	0.07	0.13	0.15	0.11	0.00	0.00	0.00	0.21	0.18	0.00	0.11	0.00	0.00	0.07	0.07	0.07	0.13	0.00	0.13	0.04	0.10	0.09	0.03	No	NA

Table 2: ROC Curve Stats

Click here to download Table: Table2.tif

Table 2 Summary statistics relating to the Receiver Operating Characteristic (ROC) analysis of the probability estimates shown in *table 1*, with respect to their ability to effectively predict lahar alert signals between 1st July and 31st December 2013. Grey rows indicate the matrices shown in *Fig. 10*

Area Under the Curve Statistics				
Test Result Variable(s)		Area	Standard Error[a]	*P*-Value[b]
No Antecedent Rainfall Consideration	10 Minute Peak Rainfall Intensity	0.82	0.09	0.01
	30 Minute Peak Rainfall Intensity	0.84	0.11	0.01
	60 Minute Peak Rainfall Intensity	0.75	0.12	0.06
24 Hour Antecedent Rainfall Consideration	10 Minute Peak Rainfall Intensity	0.74	0.13	0.07
	30 Minute Peak Rainfall Intensity	0.81	0.12	0.02
	60 Minute Peak Rainfall Intensity	0.69	0.12	0.14
3 Day Antecedent Rainfall Consideration	10 Minute Peak Rainfall Intensity	0.71	0.13	0.11
	30 Minute Peak Rainfall Intensity	0.75	0.12	0.07
	60 Minute Peak Rainfall Intensity	0.64	0.14	0.31
5 Day Antecedent Rainfall Consideration	10 Minute Peak Rainfall Intensity	0.71	0.13	0.11
	30 Minute Peak Rainfall Intensity	0.87	0.09	0.01
	60 Minute Peak Rainfall Intensity	0.89	0.08	0.00
7 Day Antecedent Rainfall Consideration	10 Minute Peak Rainfall Intensity	0.54	0.17	0.75
	30 Minute Peak Rainfall Intensity	0.82	0.10	0.02
	60 Minute Peak Rainfall Intensity	0.78	0.12	0.04
Overall Mean		0.83	0.09	0.01
"No Antecedent Rainfall" Mean		0.85	0.09	0.01
Antecedent Rainfall Mean (All Timescales)		0.81	0.10	0.02
24 Hour Antecedent Rainfall Mean		0.76	0.12	0.05
3 Day Antecedent Rainfall Mean		0.76	0.12	0.05
5 Day Antecedent Rainfall Mean		0.89	0.08	0.00
7 Day Antecedent Rainfall Mean		0.77	0.12	0.05
10 Minute Peak Rainfall Intensity Mean		0.71	0.13	0.10
30 Minute Peak Rainfall Intensity Mean		0.83	0.09	0.01
60 Minute Peak Rainfall Intensity Mean		0.79	0.10	0.02

a. Under the nonparametric assumption

b. Null hypothesis: true area = 0.5.

Table 3: Peak Probability Timing Table
Click here to download Table: Table3.tif

Table 3 Analysis of the additional warning time that is provided by the various probability matrices when applied to the eight lahar alert signal producing events between 1st July and 31st December 2013. The time-scale of the antecedent rainfall consideration is not considered in this table as it only impacts the magnitude of the peak probability and has no effect upon its timing

Lahar Alert Signal Date	Lahar Alert Signal Start Time	Time of Max 10 Minute Peak Rainfall Intensity Based Probability With No Antecedent Rainfall Consideration	Net Time	Time of Max 30 Minute Peak Rainfall Intensity Based Probability With No Antecedent Rainfall Consideration	Net Time	Time of Max 60 Minute Peak Rainfall Intensity Based Probability with No Antecedent Rainfall Consideration	Net Time	Time of Max Antecedent Rainfall & 10 Minute Peak Rainfall Intensity Based Probability	Net Time	Time of Max Antecedent Rainfall & 30 Minute Peak Rainfall Intensity Based Probability	Net Time	Time of Max Antecedent Rainfall & 60 Minute Peak Rainfall Intensity Based Probability	Net Time	Mean Warning Time Per Event
09/07/13	14:15	13:23	00:52	13:33	00:42	14:05	00:10	13:23	00:52	13:33	00:42	13:23	00:52	00:41
15/07/13	23:50	22:52	00:58	23:50	00:00	23:12	00:38	23:50	00:00	23:50	00:00	23:17	00:33	00:21
31/08/13	15:35	15:26	00:09	15:35	00:00	15:35	00:00	15:35	00:00	15:35	00:00	15:35	00:00	00:01
17/09/13	01:25	00:05	01:20	01:15	00:10	01:10	00:15	00:05	01:20	01:15	00:10	00:50	00:35	00:38
29/09/13	10:25	09:51	00:34	09:56	00:29	09:51	00:34	09:51	00:34	09:56	00:29	10:01	00:24	00:30
17/11/13	18:35	18:35	00:00	18:35	00:00	18:35	00:00	18:35	00:00	18:35	00:00	18:35	00:00	00:00
26/11/13	22:10	21:50	00:20	21:50	00:20	21:50	00:20	21:35	00:35	21:35	00:35	21:40	00:30	00:26
20/12/13	05:05	04:30	00:35	04:30	00:35	04:35	00:30	04:20	00:45	04:20	00:45	04:25	00:40	00:38
Mean Warning Time Provided Per Matrix Type			00:36		00:17		00:18		00:30		00:20		00:26	